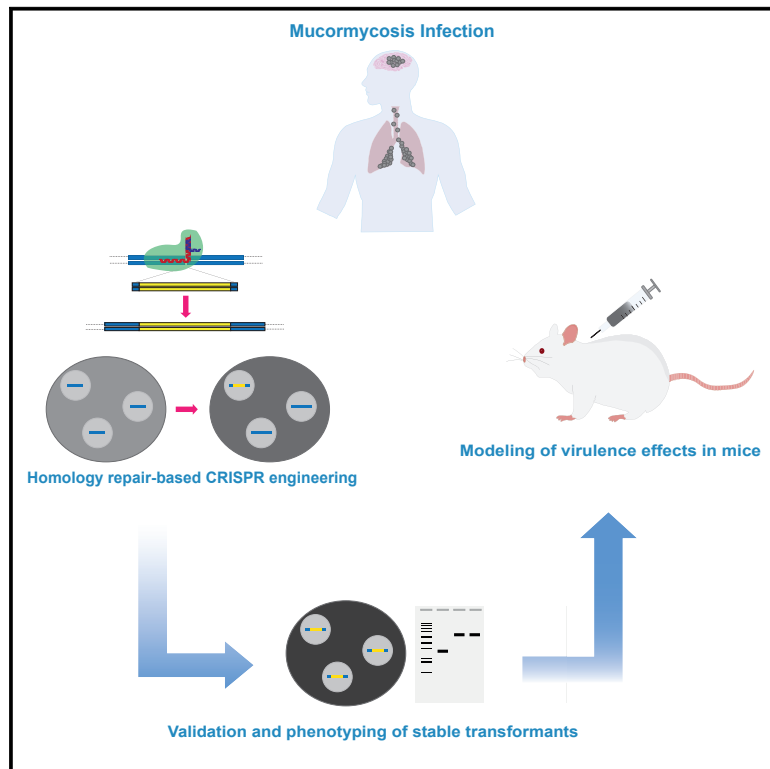


Stable and reproducible homologous recombination enables CRISPR-based engineering in the fungus *Rhizopus microsporus*

Graphical abstract



Authors

Carlos Lax,
 María Isabel Navarro-Mendoza,
 Carlos Pérez-Arques, Eusebio Navarro,
 Francisco Esteban Nicolás,
 Victoriano Garre

Correspondence

fnicolas@um.es (F.E.N.),
 vgarre@um.es (V.G.)

In brief

Lax et al. establish a procedure for genetic manipulation of the fungus *Rhizopus microsporus*, one of the main causal agents of mucormycosis. Stable homologous recombination enables editing through CRISPR-Cas9 and microhomology repair templates. Stable, homokaryotic mutants are generated and tested with virulence assays in immunocompromised mice.

Highlights

- Isolates and characterizes a mutagen-free recipient *R. microsporus* strain
- Establishes and optimizes the conditions for protoplast transformation
- Establishes a CRISPR-based procedure to generate stable homokaryotic mutant strains
- Tests the virulence of the generated mutant strains in immunocompetent mice



Report

Stable and reproducible homologous recombination enables CRISPR-based engineering in the fungus *Rhizopus microsporus*

Carlos Lax,¹ María Isabel Navarro-Mendoza,² Carlos Pérez-Arques,² Eusebio Navarro,¹ Francisco Esteban Nicolás,^{1,*} and Victoriano Garre^{1,3,*}

¹Departamento de Genética y Microbiología, Facultad de Biología, Universidad de Murcia, 30100 Murcia, Spain

²Department of Molecular Genetics and Microbiology, Duke University Medical Center, Durham, NC 27710, USA

³Lead contact

*Correspondence: fnicolas@um.es (F.E.N.), vgarre@um.es (V.G.)

<https://doi.org/10.1016/j.crmeth.2021.100124>

MOTIVATION Due to increasing cases of the fatal fungal disease mucormycosis, including cases associated with COVID-19 patients, there is an urgent need to improve genetically tractable models of the causative fungal species. Genetic manipulation tools are available in *Mucor lusitanicus*, but this species shows low virulence and is therefore not the ideal model. Our goal was to develop tools for genetic manipulation of *Rhizopus microsporus*, because it is a virulent and frequently causative agent of mucormycosis and has also been used to model interactions between Mucorales and endobacteria. With our methodology, which combines the use of CRISPR-Cas9 and microhomology DNA templates, we have achieved stable targeted integrations by homologous recombination. This has allowed us to analyze the first visual phenotypes in *R. microsporus* caused by gene disruption and to discover a possible role for the *pyrF* gene in virulence. Considering these newly developed genetic tools, we propose *R. microsporus* as a model to study virulence and molecular genetics in the mucormycosis field.

SUMMARY

Mucormycosis is a lethal and emerging disease that has lacked a genetic model fulfilling both high virulence and the possibility of performing stable and reproducible gene manipulation by homologous recombination (HR). Here, we developed a new methodology to successfully perform HR in *Rhizopus microsporus*. We isolated an uracil auxotrophic recipient strain and optimized the critical steps in the genetic transformation of this fungus. This was followed by an adaptation of a plasmid-free CRISPR-Cas9 system coupled with microhomology repair templates. We reproducibly generated stable mutants in the genes *leuA* and *crgA*, encoding a 3-isopropylmalate dehydratase and an ubiquitin ligase, respectively. Our new genetic model showed that mutations in the gene *pyrF*, a key virulence gene in several bacterial and fungal pathogens, correlated with an avirulent phenotype in an immunocompetent murine host. This was reverted by gene complementation, showing the broad possibilities of our methodology.

INTRODUCTION

The Mucorales is a group of early-diverging fungi with many distinct and unique features that has been scarcely studied due to the reluctance to be genetically transformed (Obraztsova et al., 2004). The interest in the study of Mucorales has increased because of the renewed emergence of the fungal infectious disease known as mucormycosis. Mucormycosis is a lethal disease caused by several mucoralean species, being the most frequent among the genus *Rhizopus*, followed by *Mucor* and *Lichtheimia* (Alvarez et al., 2009; Cornely et al., 2019; Roden et al., 2005). In the past, mucormycosis was considered a rare infection

affecting immunosuppressed and otherwise compromised patients. However, new clinical reports and improvements in the correct diagnosis of mucormycosis have shown an emerging increase in the number of cases (Chayakulkeeree et al., 2006; Kontoyiannis, 2017). Indeed, the increased incidence of mucormycosis in COVID-19 patients associated with steroid treatment has arisen the concerns of the scientific and clinical community to treat infections caused by the named black fungus (John et al., 2021; Veisi et al., 2021). More importantly, an escalating number of mucormycosis cases has been reported in healthy patients without known predisposing diseases (Prakash and Chakrabarti, 2019; Sridhara et al., 2005). Mucormycosis has mortality rates



that can reach 90% in the cases of bloodstream-disseminated infection (Hassan and Voigt, 2019; Jeong et al., 2019). These high mortality rates are mainly due to the innate antifungal drug resistance of Mucorales, which leaves clinicians with a few poorly effective treatments against mucormycosis (Caetano et al., 2019; Caramalho et al., 2017; Cornely et al., 2019; Danaoui, 2017; Luo et al., 2013; Maurer et al., 2015). In addition, Mucorales can rapidly acquire new antifungal drug resistance through an exclusive RNAi-based mechanism to quickly and temporally generate resistant epimutants (Calo et al., 2014). In this sense, most of the current studies in Mucorales are focused on investigating new genes, pathways, methodologies, and virulence factors that might be the targets for future antifungal developments against mucormycosis (Binder et al., 2018; Gebremariam et al., 2019; Lax et al., 2020; López-Fernández et al., 2018; López-Muñoz et al., 2018; Navarro-Mendoza et al., 2018; Pérez-Arques et al., 2019, 2021a, 2021b; Trieu et al., 2017).

In the study of mucormycosis, the difficulty of the genetic transformation and manipulation of the Mucorales species has a remarkable exception: the fungus *Mucor lusitanicus*, previously known as *Mucor circinelloides* f. *lusitanicus* (Wagner et al., 2020). Hundreds of genes have been successfully interrupted or replaced by homologous recombination (HR) in this fungus. In addition, other genetic tools such as plasmid transformation, RNAi induction, genetic complementation, directed mutagenesis, and gene tagging are also available in *M. lusitanicus* (Navarro-Mendoza et al., 2019; Nicolas et al., 2003; Trieu et al., 2015, 2017). These tools have allowed the genetic study of many cellular processes in Mucorales, including the light responses, the RNAi mechanism, and more recently, the Mucorales pathogenesis. Unfortunately, this fungal model shows very low virulence, and infection assays only work in few specific murine strains after strong immunosuppression (Li et al., 2011) or drug-induced diabetes (Valle-Maldonado et al., 2020). In this sense, the genetic manipulation reluctance of Mucorales is limiting the research community to study mucormycosis.

Our purpose in this work is to overcome this limitation by creating a new methodology that allows stable and reproducible genetic manipulation in a Mucoral different from the *Mucor* species. We selected *Rhizopus microsporus* as a candidate model because it is one of the most frequent causal agents of mucormycosis and a well-known model to study the interaction of Mucorales with endobacteria (Mondo et al., 2017; Prakash and Chakrabarti, 2019; Skiada et al., 2011). We have optimized all the critical steps for transforming and achieving stable and reproducible genetic disruption of *R. microsporus* genes. Thus, we interrupted the gene *leuA*, creating a leucine auxotrophic strain, and *crgA*, which resulted in a pleiotropic phenotype that affected development of aerial hyphae and melanin overaccumulation, resembling the pleiotropic phenotype observed in the *M. lusitanicus* *crgA* mutant, suggesting conservation of the *crgA* function in Mucorales. Finally, we established a virulence assay that uses immunocompetent mice that revealed that uracil biosynthesis is essential for full virulence in *R. microsporus*. This work may be a milestone in the study of mucormycosis, as it provides a new study model that combines complete virulence robustness and capacity for proper genetic manipulation.

RESULTS

Spontaneous uracil auxotrophic strain isolation

The first step for developing a transformation and gene disruption procedure for *R. microsporus* was to isolate a recipient strain with a reduced mutational burden by selecting spontaneous uracil auxotrophs. The complementation of uracil auxotrophy has been extensively used as a selective marker in the transformation of other fungi, including Mucorales (Gutiérrez et al., 2011; Ibragimova et al., 2020; Ibrahim et al., 2007; Nosheen et al., 2021). To select spontaneous mutants in uracil biosynthesis (Figure S1A), spores of the wild-type (WT) strain ATCC 11559 were inoculated in liquid-rich media (YPG) supplemented with 5-Fluoro-orotic acid (5-FOA) and with uridine. The uracil biosynthesis pathway converts 5-FOA into 5-fluorouracil, a toxic compound that inhibits growth. After 48 h of growth, the cells were plated in solid YPG media, also supplemented with 5-FOA and uridine. Twenty 5-FOA-resistant colonies were isolated (R1–R20) and inoculated in both minimal medium (YNB) with and without uridine to check uracil auxotrophy. Isolates that showed strong growth in 5-FOA and no-growth in YNB without uridine were selected as uracil auxotrophs (Figures S1A and S1B). Mutations in either the *pyrG* gene encoding the orotidine 5'-phosphate decarboxylase (JGI: 279857) or the *pyrF* gene encoding the orotate phosphoribosyl transferase (JGI: 231940) block the uracil biosynthesis (Boeke et al., 1987; Bruni et al., 2019; Ibragimova et al., 2020). Sequencing of both genes from four different auxotrophs (R1, R3, R5, and R8) revealed that two of them (R3 and R5) had a mutation in the *pyrF* gene, but not in the *pyrG* gene. The other two, R1 and R8, have no mutations in the *pyrG* or the *pyrF* genes, suggesting the presence of mutations in other genes involved in the uracil metabolism. The R3 and R5 strains carry a nucleotide substitution that results in a nonsynonymous change in position 73 (K73E) (Figure S1C), suggesting that they both derive from the same initial auxotroph. Position 73 is part of the enzyme active site (AYKG) that interacts with the substrate α -D-5-phosphoribosyl-1-pyrophosphate (PRPP) (Figures S1D and S1E) (Scapin et al., 1995), and its mutation in the *Salmonella typhimurium* enzyme produced a 50–100-fold decrease in K_{cat} and an 8–12-fold increase in the PRPP K_M (Ozturk et al., 1995). Based on these results, we selected the R3, thereafter named UM1, as the recipient strain for further experiments.

Optimized conditions for protoplast generation

A transformation protocol for Mucorales requires to determine the optimal germination stage to enhance the action of the lytic enzymes and the survival of the resulting protoplasts. Fresh spores of *R. microsporus* were grown in YPG medium supplemented with uridine at different temperatures in a rotary shaker (Figure S2). Spores swelled to approximately double their size, from 4.90 ± 0.62 to 9.39 ± 0.98 μm , and generally sprouted 1–3 germ tubes per spore in the early stages. The germination stage is optimal when spores are completely swollen, and they start emitting the germ tubes (Figure S2A, framed in blue) (Nicolás et al., 2018). The time required for germination decreased as the temperature increased (Figure S2). Although germination was faster at 37°C (between 3 and 3.5 h), the viability of the

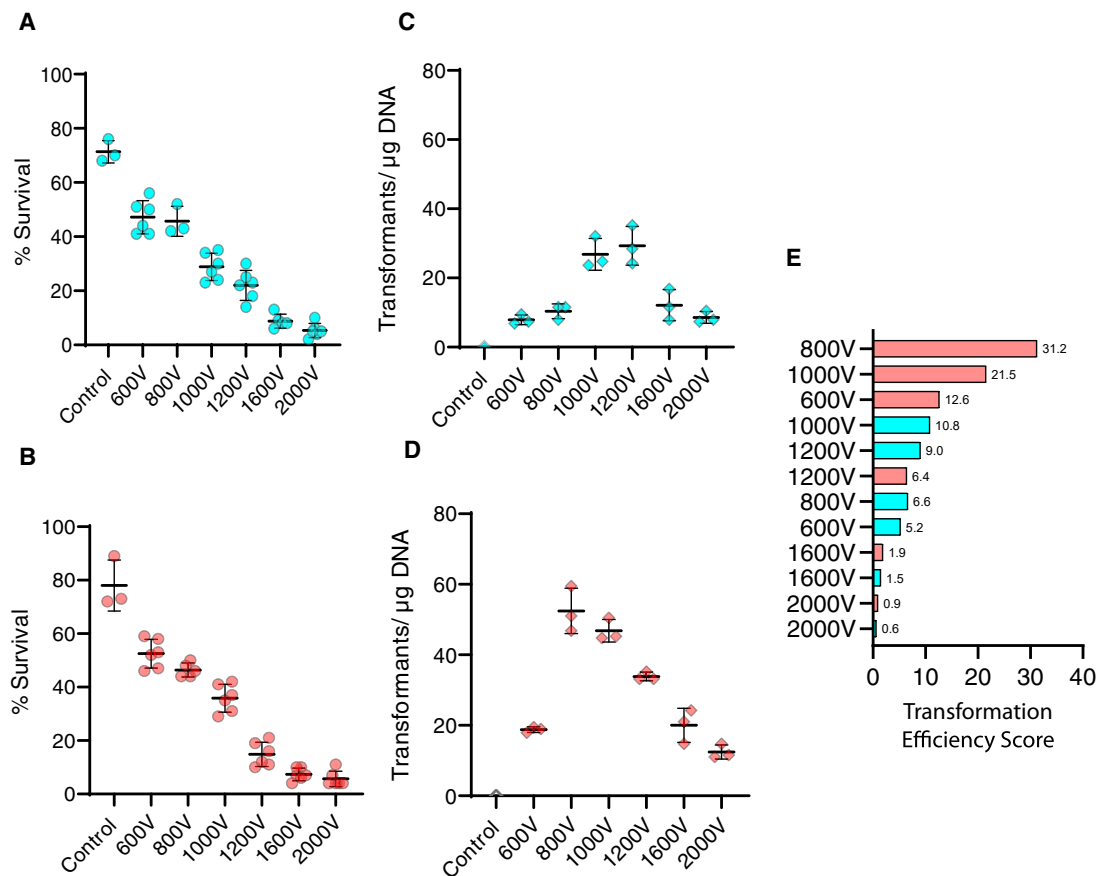


Figure 1. Transformation efficiency and survival rate of electroporated protoplast of the UM1 strain

(A and B) The survival rate of the UM1 protoplast after electroporation after different ED (A) and TC pulses (B). Data is represented as mean \pm SD. Each point corresponds to a different plate with 200 protoplasts (2 plates/cuvette).

(C and D) Transformation rate obtained after ED (C) and TC pulses (D). Data is represented as mean \pm SD. Each point corresponds to a different electroporation cuvette.

(E) Transformation efficiency score was obtained as the product of the average transformants/ μ g of DNA and the average survival rate (normalized considering 1 as the value of the survival rate of the negative control).

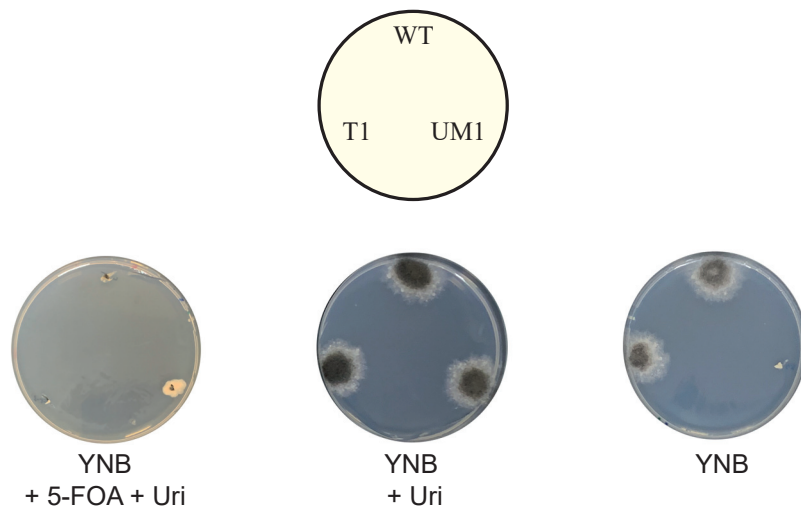
protoplasts was more affected at this temperature than 26°C and 33°C, as determined by direct protoplast observation and preliminary viability tests (Figure S2B). Therefore, 33°C and 4.5 h were selected as the germination conditions for further experiments. Following the procedures established in other fungi, we tested increasing concentrations of a combination of lysing enzymes from *Trichoderma harzianum* and chitosanase from *Streptomyces griseus* until convenient lysis was observed, when cells were subjected to a hypotonic shock (de Bekker et al., 2009; Gruber et al., 1990; Gutiérrez et al., 2011). We concluded that with a combination of 3 mg of lysing enzymes and 0.0008 units of chitosanase per 1×10^7 spores, the cell wall degradation was optimal, and the protoplast viability was not exceedingly affected, as we ascertained in the next steps.

Electroporation and efficient transformation of *R. microsporus* protoplasts

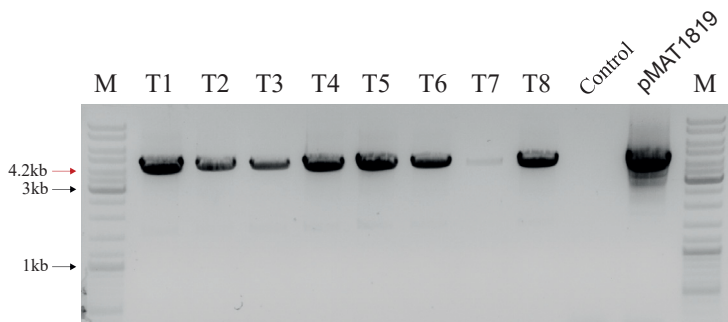
To establish the electroporation parameters, protoplasts of the uracil auxotroph UM1 were transformed with a self-replicative

plasmid containing *R. microsporus pyrF* gene (pMAT1819). We tested two different electroporation methods: exponential decay pulse (ED) and time constant pulse (TC). ED starts with the set voltage and rapidly decays (exponentially) to zero. This method was successfully applied to *M. lusitanicus* and several other fungal species (Escoffre et al., 2009; Gutiérrez et al., 2011). On the other hand, the TC method supposes a continuous pulse of a set voltage during a set time (Escoffre et al., 2009). The survival rate and the transformation efficiency were tested at 600, 800, 1000, 1200, 1600, and 2000 V for both ED and TC pulses. For TC pulses, time was set to 5 milliseconds (ms), because preliminary tests with different time pulses showed that the highest transformation efficiency was in the range of 5–7 ms (Figure S3). For ED pulses, capacitance and resistance were set to 25 μ F and 400 Ω , respectively, following the well-established protocol for *M. lusitanicus* (Gutiérrez et al., 2011). The results showed decreased survival rates for both ED and TC pulses as the voltage increased (Figures 1A and 1B). Survival rates ranged from 40% to 60% (compared with the negative control) at lower

A



B



voltages (600–800 V) to ~10% for higher voltages (1600–2000 V). In ED pulses, the highest transformation rates were obtained at 1000–1200 V with approximately 30 transformants/ μg of DNA, whereas higher and lower voltages produced less than 20 transformants/ μg of DNA (Figure 1C).

Interestingly, for TC pulses, a higher transformation rate was obtained, especially at 800 V and 1000 V, which nearly doubled the best of the ED pulses with approximately 50 transformants/ μg of DNA (Figure 1D). Analysis of the transformation efficiency scores revealed that the 800 V TC pulse was the best condition. The transformants obtained were able to grow without uridine supplementation in minimal media but unable to grow in the presence of 5-FOA, like the WT strain and unlike the recipient strain UM1 (Figure 2A). The presence of the plasmid in the transformants, verified by PCR analysis in eight randomly selected transformants (Figure 2B), confirmed the success of this transformation method.

Stable disruption of *crgA* and *leuA* genes by CRISPR-Cas9 and HR

Once *R. microsporus* transformation using a plasmid was achieved, we set up a procedure to disrupt target genes using a plasmid-free CRISPR-Cas9 system and HR-mediated DNA repair (Figure 3A) with microhomology templates (from 30 to 50 base

Figure 2. Characterization of the transformants generated with the pMAT1819 plasmid

(A) Growth of the *R. microsporus* wild type strain ATCC 11559 (WT), UM1 strain, and a UM1 transformant-carrying plasmid pMAT1819 that complemented uracil auxotrophy (T1) on YNB medium supplemented with 5-FOA (3 g/L) and uridine (200 mg/L) (left), YNB medium supplemented with uridine (200 mg/L) (middle), and YNB medium (right). (B) DNA was extracted from eight randomly selected transformants (T1–T8) and amplified by PCR using the M13_F and M13_R primers that bind to the vector sequence flanking the *pyrF* gene in plasmid pMAT1819. PCR amplification with the same primers of DNA from the untransformed UM1 strain and the purified plasmid served as negative and positive controls, respectively. Red arrow points to the expected amplification fragment. Black arrows point to the indicated bands of the marker.

pairs [bp]). These templates were generated by PCR amplification of the *pyrF* locus with primers that included short tails corresponding to sequences flanking the cleavage site of a guided Cas9. For this approach, we reduced the *pyrF* gene length from 4.2 to 3.4 kb because the transformation rate was unaffected in transformations with self-replicative plasmids.

We tested this strategy by disrupting two different genes: *crgA* (JGI: 226533) and *leuA* (JGI: 228594). *crgA* is the predicted homolog to the *M. lusitanicus* *crgA* gene, which encodes a ubiquitin ligase that re-

presses carotenogenesis, sporangiophore length, and sporulation by inactivating an activator of the light response of this fungus (Navarro et al., 2013; Nicolas et al., 2008; Silva et al., 2008). For its part, *leuA* is the predicted homolog to *M. lusitanicus* *leuA* gene that codes for a 3-isopropylmalate dehydratase, involved in leucine biosynthesis (Roncero et al., 1989). We designed two different guide RNAs (gRNAs) (gRNA1 and gRNA2) for each gene, targeting different sequences, and the corresponding HR templates (Table S1). These templates consisted of the 3.4-kb *pyrF* gene flanked by 38-bp sequences complementary to the 5' and 3' regions adjacent to the predicted Cas9 cleavage site. *In vitro* assembled ribonucleoprotein (RNP) complexes formed by the Cas9 and a gRNA, together with the corresponding templates, were used to transform the UM1 strain. The transformation efficiency was reduced compared with plasmid transformation and varied among the different combinations of gRNA and templates (Table 1). *In vitro* cleavage activity assays of each gRNA-Cas9 and template combination revealed that transformation efficiency correlates with *in vitro* cleavage efficiencies (Figure S4). Thus, when the Cas9 loaded with *leuA*_gRNA1 was incubated with a *leuA* fragment, the amount of uncut DNA was higher than when *leuA*_gRNA2 was used. Correspondingly, this second gRNA yielded approximately double the number of transformants/ μg of DNA (Table 1). To confirm a proper *pyrF*

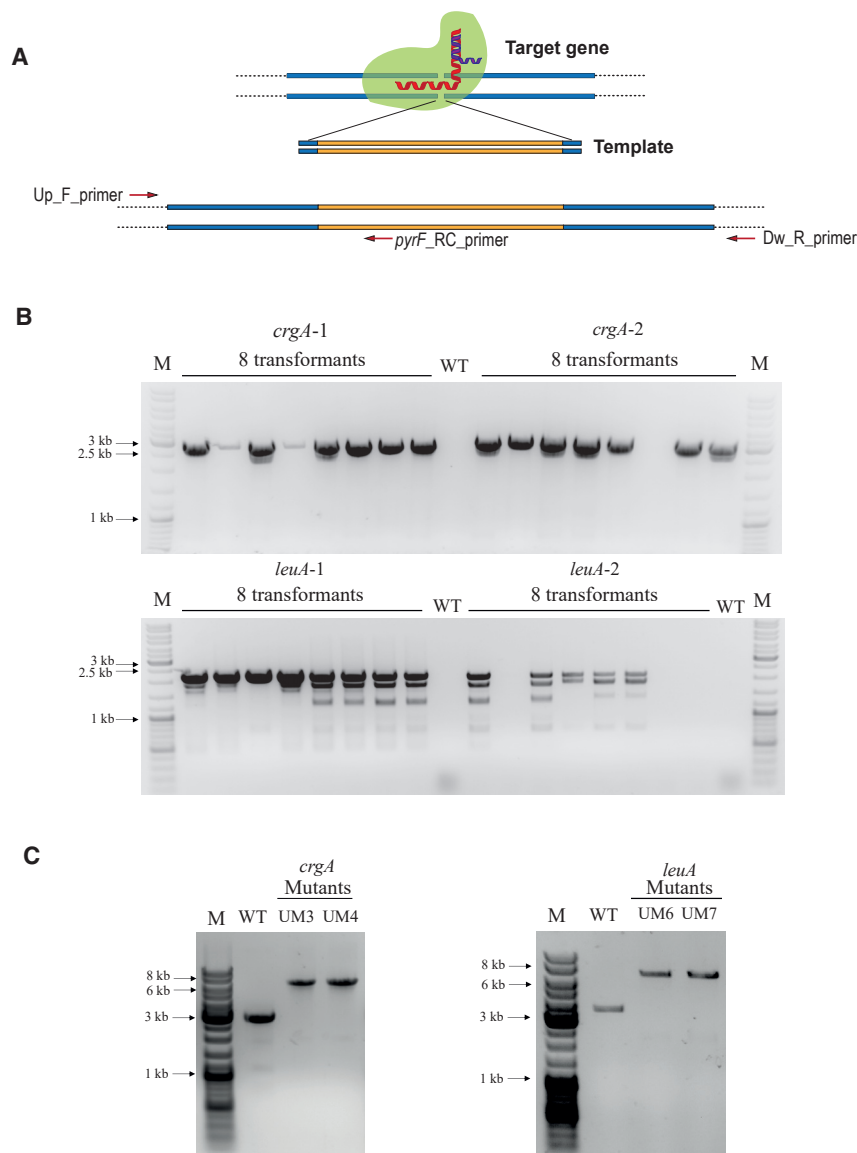


Figure 3. Disruption of *crgA* and *leuA* genes

(A) Strategy followed to disrupt target genes with the combination of gRNA-Cas9 complex and a designed DNA template. Positions of the primers used to check gene disruption and homokaryosis are also shown.

(B) Gene disruption validation by PCR using the Up_F primer and the *pyrF*_RC primer for eight randomly selected transformants obtained with *crgA*_gRNA1 + *crgA*Template1 (expected fragment of 2.8 kb), *crgA*_gRNA2 + *crgA*Template2 (expected fragment of 2.9 kb), *leuA*_gRNA1 + *leuA*Template1 (expected fragment of 2.1 kb), and *leuA*_gRNA2 + *leuA*Template2 (expected fragment of 2.2 kb). DNA from the *R. microsporus* wild-type strain ATCC 11559 was used as a negative control (WT).

(C) PCR fragments smaller than the ones expected in some lanes of the *leuA* transformants corresponded to nonspecific PCR products. (C) PCR amplification of the *crgA* and *leuA* locus of the indicated transformants using the Up_F primer and the Dw_R primer. Expected PCR DNA fragments from WT and disrupted *crgA* locus were 3.1 kb and 6.6 kb in length, respectively. For *leuA*, expected PCR products from WT and disrupted locus were 3.6 kb and 7.1 kb in length, respectively. Black arrows point to the indicated bands of the marker.

loci and the only presence of PCR products 3.4 kb larger evidenced that all transformants were homokaryons for the disruption (Figure 3C). Furthermore, this result also confirmed that the integration was stable and maintained through the successive cycles of vegetative growth.

***crgA* mutants were affected in aerial mycelia development and melanin synthesis, while *leuA* disruption caused leucine auxotrophy**

The phenotype of the mutants was analyzed to elucidate the function of

integration at the target site, we analyzed the targeted loci of 16 randomly selected transformants obtained from each transformation (32 for each gene) by PCR using the gene-specific Up_F primer and *pyrF*_R primer. Thus, a total of 64 transformants were checked for integration in the targeted regions (Figures 3A and 3B show representative gels with eight transformants for each gRNA). The correct integration ranges from 62.5% to 96.9% depending on the gRNA (Table 1), proving the high reliability of this method to perform targeted integration and gene disruption. As *R. microsporus* has multinucleated spores, initial transformants were expected to be heterokaryons, and therefore, two initial transformants for the disruption of *crgA* and *leuA* genes (UM3 and UM4 for *crgA* and UM6 and UM7 for *leuA*) were grown for 4–5 vegetative cycles in minimal medium, and the targeted loci were analyzed by PCR using the corresponding Up_F primers and the Dw_R primers. The absence of the PCR products corresponding to the WT *crgA* and *leuA*

crgA and *leuA* in *R. microsporus*. The radial growth and spore production of two different *crgA* mutants (UM3 and UM4), one from each gRNA + template combination, was similar to the WT strain (Figure S5). However, the mutants showed a clear defective development of aerial mycelium similar to the *crgA* null mutant of *M. lusitanicus* (Figure 4A). The mutant *M. lusitanicus* also shows a dark-yellow color caused by the overproduction of beta carotene (Navarro et al., 2001; Nicolas et al., 2008), which cannot be observed in *R. microsporus* because it lacks colored carotenoids. However, *R. microsporus* *crgA* mutants showed a dark brown color that could be associated with melanin overaccumulation (Figures 4A and 4B). Thus, we analyzed the melanin levels in extracts of the WT and mutants by measuring absorbance (Gupta and Chattoo, 2007; Saha et al., 2020). The absorbance at 405 nm was 1.92-fold higher in the *crgA* mutant than in the WT strain (Figure 4C), suggesting *crgA* mutant overaccumulated melanin. Regarding the

Table 1. Results of transformations for *crgA* and *leuA* genes using CRISPR-Cas9

	<i>crgA_g1 crgA_Template1</i>	<i>crgA_g2 crgA_Template2</i>	<i>leuA_g1 leuA_Template1</i>	<i>leuA_g2 leuA_Template2</i>
Transformants/ μ g DNA	23.32 \pm 5.17	32.89 \pm 2.66	13.82 \pm 1.15	27.76 \pm 0.19

phenotype of *leuA* mutants, we plated all the mutants confirmed by PCR in minimal YNB medium with and without leucine supplementation. Unlike the WT strain, *leuA* mutants were unable to grow without the presence of leucine (Figure 4D), evidencing the loss of gene function.

Testing the pathogenic potential of genetically modified strains from *R. microsporus*. Endogenous uracil production is essential for virulence

The capacity to genetically modify *R. microsporus* opened a whole range of genetic engineering possibilities in this fungus. However, our main goal was to generate a new genetic model to study mucormycosis. Thus, we tested the mutants *crgA::pyrF* (UM3) and *leuA::pyrF* (UM6) in a survival assay using a murine model in which the fungal spores were intravenously injected (Figure 4E). Instead of using immunosuppressed mice as with *M. lusitanicus*, we employed the common murine strain Swiss without immunosuppression treatment. Spores of the mutants in *crgA* and *leuA* genes caused rapid death of all mice between 6 and 7 days post-injection, similarly to the WT strain. However, spores of the *pyrF* mutant did not kill any mice, showing a complete avirulent phenotype. The virulent phenotype of the *crgA* and *leuA* mutants demonstrated that the lack of function of *pyrF* was utterly rescued in these mutants by the ectopic expression of the *pyrF* integrated in those loci, indicating that gene complementation was also successful in the genetic model of *R. microsporus*. It is worthy of noting that our results showed that genetically modified strains of *R. microsporus* could be easily tested for their pathogenic potential. Other mucormycosis models require immunosuppression before and during the infection assays or the use of neutropenic strains; thus, our strategy proposes a cost-effective and efficient virulence assay method.

DISCUSSION

Genetic transformation of Mucorales has always been an obstacle hampering the study of these early-diverging fungi. Several attempts of genetic transformation of different species did not thrive in the long term. One example is *Rhizopus delemar*, another highly frequent isolated causal agent from mucormycosis patients (Prakash and Chakrabarti, 2019). An attempt to disrupt the gene *ptr1*, coding for a ferroxidase involved in the high-affinity iron uptake by double crossover HR generates only one heterokaryotic mutant strain that failed to segregate homokaryons (Ibrahim et al., 2010). Other studies used the CRISPR-Cas9 system to induce directed mutagenesis in a selective marker by the nonhomologous end-joining repair mechanism after a double-strand break caused by the guided Cas9 enzyme. This CRISPR-Cas9 system was used in *R. delemar* and *Lichtheimia corymbifera*, another frequent causal agent of mucormycosis, to mutate genes *pyrF* and *pyrG*, respectively, selecting for 5-FOA resistance (Bruni et al., 2019; Ibragimova et al., 2020). The main drawback of this strategy is that the mutagen-

esis can be exclusively directed to genes with a selective method such as the 5-FOA resistance, which makes it impossible to widen it to the whole genome. Another strategy to genetically manipulate Mucorales is the transformation with self-replicative plasmids, first achieved in *M. lusitanicus* and, later, in *R. delemar* and *L. corymbifera* (Benito et al., 1995; Bruni et al., 2019; Ibragimova et al., 2020). These plasmids have been used to manipulate gene expression through the RNAi mechanism (Bruni et al., 2019; Ibragimova et al., 2020; Ibrahim et al., 2010; Soliman et al., 2021). The main problem of the self-replicative plasmids is that they do not replicate in all the nuclei of multinucleated and coenocytic hyphae. During nuclei segregation and sporulation, only a variable proportion of the descendant spores contains some nucleus-carrying plasmids (Nicolas et al., 2003). Moreover, among the subpopulation that receives the plasmid, only those with a high number of plasmid copies can trigger the RNAi mechanism (Nicolas et al., 2003).

Stable and reproducible gene disruption by HR in Mucorales has been only achieved in *Mucor*, particularly *M. lusitanicus* (Navarro et al., 2001). Consequently, other derived genetic tools were also developed in this fungus, such as gene overexpression (Pérez-Arques et al., 2021a), complementation (Trieu et al., 2015), and protein tagging (Navarro-Mendoza et al., 2019). During the last decade, this fungus has served as the unique model with a wide repertoire of genetic engineering tools in the urgent search for new target genes that are involved in Mucorales pathogenesis (Lax et al., 2020; Li et al., 2011; Trieu et al., 2017; Navarro-Mendoza et al., 2018; Pérez-Arques et al., 2019, 2021b; López-Fernández et al., 2018; Patiño-Medina et al., 2018, 2019). However, *M. lusitanicus* shows reduced virulence, and survival assays can only be done in the specific mouse strains following rigorous immunosuppression (Li et al., 2011).

In this scenario, understanding of Mucorales pathogenesis urgently requires a genetic model that unifies the genetic amenability of *M. lusitanicus* and high virulence. Here, we developed a new genetic model of mucormycosis based on *R. microsporus* and the methodology to transform it and generate stable mutants in target genes. First, we developed a new procedure to obtain spontaneous uracil auxotrophic strains that resulted in the isolation of a strain mutated in the *pyrF* gene that can be used as a recipient in transformation experiments. As this strain is a spontaneous mutant, it is expected that it carries a low mutational burden, reducing the likelihood that additional mutations in the genome negatively affect fitness and virulence, which could interfere with genetic studies of new potential virulence factors.

Since the implementation of *M. lusitanicus* as a model for HR-mediated genetic manipulations in Mucorales, the methodology to transform this species has been optimized several times (Gutiérrez et al., 2011; van Heeswijk and Roncero, 1984; Nicolás et al., 2018; Trieu et al., 2017; Vellanki et al., 2018), providing knowledge about the critical steps that must be carefully taken to ensure a successful transformation. In this work, those essential steps were optimized for *R. microsporus*, finding that this fungus

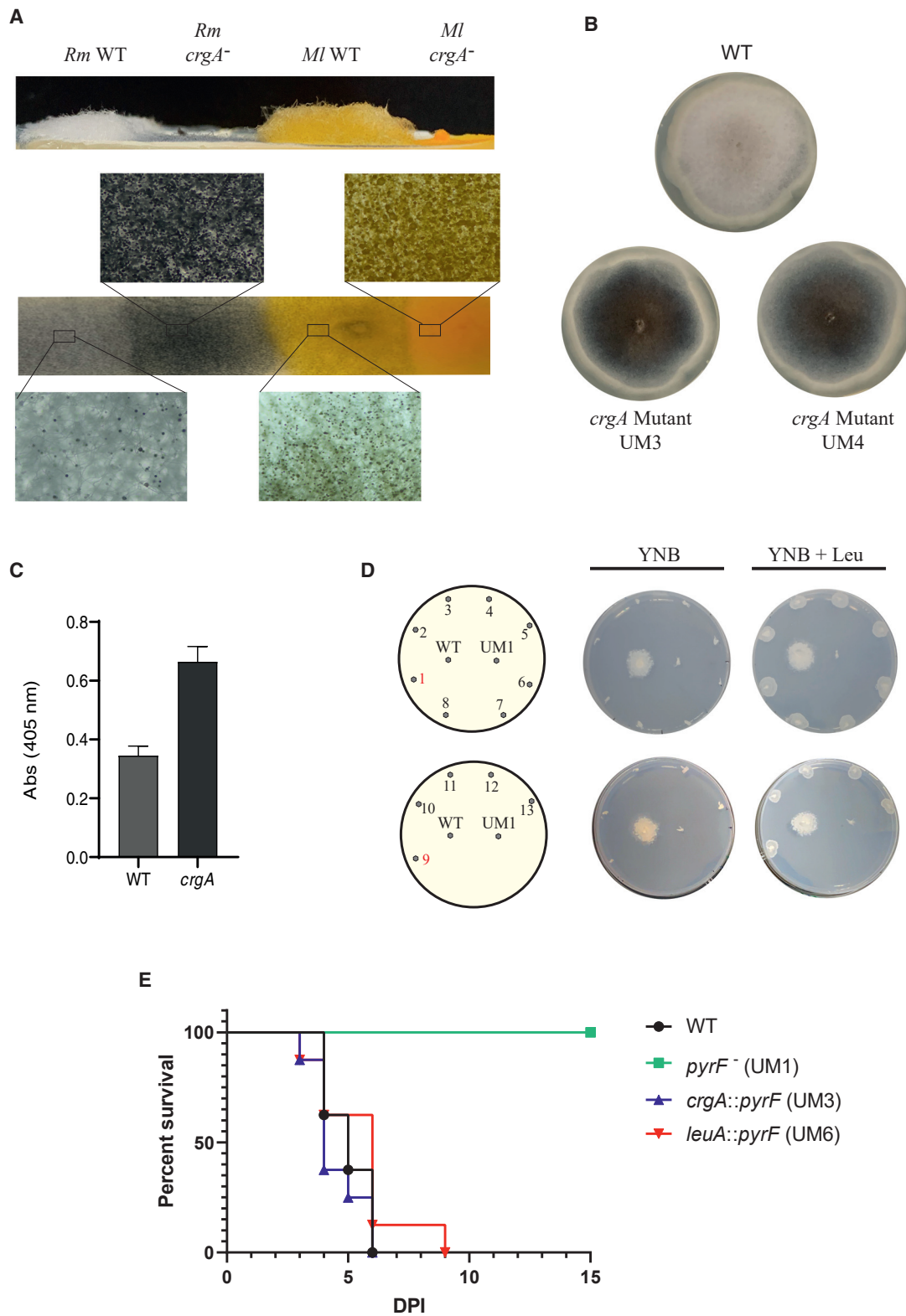


Figure 4. Phenotypic effects of *crgA*- and *leuA*-targeted disruption

(A) Aerial mycelium and mycelial color of *R. microsporus* WT strain, an *R. microsporus crgA* mutant, *M. lusitanicus* WT strain (CBS 277.49), and an *M. lusitanicus crgA* mutant.

(legend continued on next page)

requires specific conditions in all the critical steps. Thus, *R. microsporus* germinates faster than *M. lusitanicus* at higher temperatures, which might be related to its higher virulence (Bhabhra and Askew, 2005). After germination, the digestion of *R. microsporus* needs higher concentrations of lysing enzymes and chitosanase than *M. lusitanicus*, indicating a more robust cell wall. The cell wall differences might also be behind the improvement in the electroporation efficiency after changing the pulse method. Finally, the use of a plasmid-free CRISPR-Cas9 system definitively ensured HR, which is a highly specific gene targeting system in fungi (Abdallah et al., 2018). We showed that a template DNA containing upstream and downstream homologous tails of only 38 bp was enough to disrupt the target gene (Yuzbashev et al., 2015). This represents an advantageous manner of generating the recombinant constructs for HR, because they can be produced by PCR using affordable long primers with the corresponding saving of time and effort, compared with the construction of DNA fragments with longer arms (Abdallah et al., 2017; Yuzbashev et al., 2015). By using this methodology, we generated homokaryotic and stable mutants in two genes of *R. microsporus*. The gene *leuA*, ortholog of the *M. lusitanicus leuA* gene, was selected to generate a second auxotrophic strain that will be helpful in future studies requiring the functional analysis of two genes. The second gene, *crgA*, was selected because of its pleiotropic and striking visual phenotype in mutants of its putative ortholog in *M. lusitanicus*. The lack of *crgA* in *M. lusitanicus* induces the overaccumulation of carotenoids, resulting in dark-yellow mycelium (Navarro et al., 2001; Nicolás-Molina et al., 2008). This visual phenotype in *M. lusitanicus* is pronounced by the lack of aerial sporangiophores, a phenotype also found in the *crgA* mutants of *R. microsporus*. *R. microsporus* does not accumulate colored carotenoids, but disruption of *crgA* provokes black-colored mycelia after sporulation as a result of an overaccumulation of melanin. Carotenoids and melanin are secondary metabolites produced after the initial growth phase. The fact that melanin is overaccumulated in *crgA* mutants suggests that *crgA* has evolved in *R. microsporus* to regulate melanin biosynthesis in a similar manner as carotenoids biosynthesis in *M. lusitanicus* (Silva et al., 2008).

The lack of aerial sporangiophores and the overaccumulation of melanin are the first visual phenotypes obtained by gene disruption in a Mucoral other than *M. lusitanicus*. However, the results of the survival assays made in this work are even more relevant for the future impact of *R. microsporus* as a new genetic model for the study of mucormycosis. The WT strain, the spontaneous *pyrF* auxotrophic strain, and the two generated mutants showed expected results for typical performance in a murine

survival assay. The WT strain killed the mice rapidly and without the necessity of a previous and continued immunosuppression treatment, an important advantage over *M. lusitanicus*. Despite the pleiotropic effect provoked by disruption of *crgA* in *R. microsporus*, the virulence of the *crgA* mutant suggests that none of the regulatory pathways controlled by this gene are involved in the pathogenic potential of Mucorales. The lack of melanin correlates with a decreased virulence in other Mucorales (Soliman et al., 2020), but its overaccumulation has not been analyzed. Full virulence of the *crgA* mutant suggests that melanin overaccumulation does not increase virulence, although we cannot discard a compensatory effect on virulence by the diverse pathways altered in the *crgA* mutant. Regarding the mutants in the gene *leuA*, the virulent phenotype was equal to the WT strain, results that are similar to those previously observed for leucine auxotroph in *M. lusitanicus* (Li et al., 2011), confirming that this auxotrophy does not affect virulence in Mucorales. However, auxotrophy for uracil provoked a complete avirulent phenotype in *R. microsporus*. These findings are consistent with the result in other fungi, such as *Aspergillus fumigatus* and *Candida albicans*, whose uracil auxotrophs also present reduced virulence (Bain et al., 2006; Brand et al., 2004; D'Enfert et al., 1996). Likely, the free uridine/uracil in the tissues of the host is not enough to keep a regular fungal growth (D'Enfert et al., 1996). The tandem of controls, positive and negative, corresponding to the WT and uracil auxotrophic strains, will represent an invaluable tool for future virulence analyses in *R. microsporus*.

In summary, we have achieved stable and efficient HR-mediated genetic modification in *R. microsporus* using a plasmid-free CRISPR-Cas9 method. It is first achieved in a highly prevalent causal agent of mucormycosis and represents the second mucoralean genus that can be genetically modified stably and efficiently. Mucormycosis is currently a lethal, emerging, virulent, and drug-resistant infectious disease, and this new genetic model will represent a landmark in the study of the molecular aspect of this disease. Moreover, we propose to export the methodology developed in this work to other mucoralean species that are models in research fields different from mucormycosis, extending the genetic and molecular studies to the whole order of Mucorales.

Limitations of the study

The methodology presented in this work allows for genetic transformation and targeted integration by HR combined with the use of the CRISPR-Cas9 technology. This has required a deep optimization of every step of the process. Some of those steps are highly specific for *R. microsporus*. For that reason, in order to apply this procedure to any other related fungal species, these

(B) Growth of *R. microsporus* wild-type strain (WT) and two *crgA* mutants (72 h, YPG media).

(C) Analysis of melanin production measured by its absorbance at 405 nm (p value of 0.0008).

(D) *leuA* mutants (1–8 from gRNA1+Template1 and 9–13 from gRNA2+Template2) after 48 h of growth on YNB media supplemented with leucine (right) and without leucine (left). Mutant growth is compared with the *R. microsporus* wild-type strain (WT) and the uridine auxotrophic strain UM1. UM6 (1) and UM7 (9) mutants are highlighted in red.

(E) Survival assays of mutant strains generated from *R. microsporus*. The survival assays were made in groups of eight immunocompetent Swiss mice, which were injected with 1×10^6 spores of the mutants *pyrF*⁻ (UM1, green), *crgA::pyrF* (UM3, blue), and *leuA::pyrF* (UM6, red). In addition, the control WT strain was also injected (black). The survival rate of the mutants *crgA::pyrF* and *leuA::pyrF* and the WT strain were compared with the avirulent mutant strain *pyrF*⁻ by a Mantel-Cox test (p value < 0.0001).

specific steps should be adapted in consequence. The possibility of targeted integration of DNA templates opens broad possibilities for the development of multiple genetic tools. Some factors such as the maximum size of DNA fragments that can be used as templates remain to be further characterized.

STAR★METHODS

Detailed methods are provided in the online version of this paper and include the following:

- KEY RESOURCES TABLE
- RESOURCE AVAILABILITY
 - Lead contact
 - Materials availability
 - Data and code availability
- EXPERIMENTAL MODEL AND SUBJECT DETAILS
- METHODS DETAILS
 - Protoplast generation and electroporation
 - Nucleic acids manipulation, amplification, and plasmid construction
 - Selection of uracil auxotrophic mutants
 - gRNA – Cas9 assembly and *in vitro* activity tests
 - Phenotypic characterization of *crgA* and *leuA* mutants
 - Microscopy imaging, data representation, and statistical analysis
 - Survival assays
- QUANTIFICATION AND STATISTICAL ANALYSIS

SUPPLEMENTAL INFORMATION

Supplemental information can be found online at <https://doi.org/10.1016/j.crmeth.2021.100124>.

ACKNOWLEDGMENTS

This work was supported by the Fundación Séneca-Agencia de Ciencia y Tecnología de la Región de Murcia, Spain (20897/PI/18). The student C.L. was funded by Spanish MICIU (FPU17/05814).

AUTHOR CONTRIBUTIONS

Methodology, C.L., M.I.N.-M., and C.P.-A.; investigation, formal analysis, visualization, writing – original draft, and writing – review & editing, C.L.; funding acquisition and resources, E.N.; conceptualization, supervision, project administration, funding acquisition, and writing – review & editing, F.E.N. and V.G.

DECLARATION OF INTERESTS

The authors declare no competing interests.

Received: June 1, 2021
Revised: September 20, 2021
Accepted: November 9, 2021
Published: December 6, 2021

REFERENCES

Abdallah, Q.A., Ge, W., and Fortwendel, J.R. (2017). A simple and universal system for gene manipulation in *Aspergillus fumigatus*: In vitro-assembled

cas9-guide RNA ribonucleoproteins coupled with microhomology repair templates. *mSphere* 2, e00446.

Abdallah, Q.A., Souza, A.C.O., Martin-vicente, A., Ge, W., and Fortwendel, J.R. (2018). Whole-genome sequencing reveals highly specific gene targeting by in vitro assembled cas9-ribonucleoprotein complexes in *Aspergillus fumigatus*. *Fungal Biol. Biotechnol.* 5, 1–8.

Alvarez, E., Sutton, D.A., Cano, J., Fothergill, A.W., Stchigel, A., Rinaldi, M.G., and Guarro, J. (2009). Spectrum of zygomycete species identified in clinically significant specimens in the United States. *J. Clin. Microbiol.* 47, 1650–1656.

Bain, J.M., Stubberfield, C., and Gow, N.A.R. (2006). Ura-status-dependent adhesion of *Candida albicans* mutants. *FEMS Microbiol. Lett.* 204, 323–328.

Benito, E.P., Campuzano, V., López-Matas, M.A., De Vicente, J.I., and Eslava, A.P. (1995). Isolation, characterization and transformation, by autonomous replication, of *Mucor circinelloides* OMP-decay-deficient mutants. *Mol. Gen. Genet.* 248, 126–135.

Bhabhra, R., and Askew, D.S. (2005). Thermotolerance and virulence of *Aspergillus fumigatus*: Role of the fungal nucleolus. *Med. Mycol.* 43, S87–93.

Binder, U., Navarro-Mendoza, M.I., Naschberger, V., Bauer, I., Nicolas, F.E., Pallua, J.D., Lass-Flörl, C., and Garre, V. (2018). Generation of a *Mucor circinelloides* reporter strain—A promising new tool to study antifungal drug efficacy and mucormycosis. *Genes (Basel)* 9, 613.

Boeke, J.D., Trueheart, J., Natsoulis, G., and Fink, G.R. (1987). [10] 5-Fluoroorotic acid as a selective agent in yeast molecular genetics. *Methods Enzymol.* 154, 164–175.

Brand, A., MacCallum, D.M., Brown, A.J.P., Gow, N.A.R., and Odds, F.C. (2004). Ectopic expression of URA3 can influence the virulence phenotypes and proteome of *Candida albicans* but can be overcome by targeted reintegration of URA3 at the RPS10 locus. *Eukaryot. Cell* 3, 900–909.

Bruni, G.O., Zhong, K., Lee, S.C., and Wang, P. (2019). CRISPR-Cas9 induces point mutation in the mucormycosis fungus *Rhizopus delemar*. *Fungal Genet. Biol.* 124, 1–7.

Caetano, L.A., Faria, T., Springer, J., Loeffler, J., and Viegas, C. (2019). Anti-fungal-resistant Mucorales in different indoor environments. *Mycology* 10, 75–83.

Calo, S., Shertz-Wall, C., Lee, S.C., Bastidas, R.J., Nicolas, F.E., Granek, J.A., Mieczkowski, P., Torres-Martinez, S., Ruiz-Vazquez, R.M., Cardenas, M.E., et al. (2014). Antifungal drug resistance evoked via RNAi-dependent epimutations. *Nature* 513, 555–558.

Caramalho, R., Tyndall, J.D.A., Monk, B.C., Larentis, T., Lass-Flörl, C., and Lackner, M. (2017). Intrinsic short-tailed azole resistance in mucormycetes is due to an evolutionary conserved amino acid substitution of the lanosterol 14 α -demethylase. *Sci. Rep.* 7, 15898.

Chang, Z., and Heitman, J. (2019). Drug-resistant epimutants exhibit organ-specific stability and induction during murine infections caused by the human fungal pathogen *Mucor circinelloides*. *mBio* 10, e02579–19.

Chayakulkeeree, M., Ghannoum, M.A., and Perfect, J.R. (2006). Zygomycosis: The re-emerging fungal infection. *Eur. J. Clin. Microbiol. Infect. Dis.* 25, 215–229.

Cornely, O.A., Alastruey-Izquierdo, A., Arenz, D., Chen, S.C.A., Dannaoui, E., Hochhegger, B., Hoenigl, M., Jensen, H.E., Lagrou, K., Lewis, R.E., et al. (2019). Global guideline for the diagnosis and management of mucormycosis: An initiative of the European confederation of medical mycology in cooperation with the mycoses study group education and research consortium. *Lancet Infect. Dis.* 19, e405–e421.

de Bekker, C., Wiebenga, A., Aguilar, G., and Wösten, H.A.B. (2009). An enzyme cocktail for efficient protoplast formation in *Aspergillus niger*. *J. Microbiol. Methods* 76, 305–306.

Dannaoui, E. (2017). Antifungal resistance in mucorales. *Int. J. Antimicrob. Agents* 50, 617–621.

D'Enfert, C., Diaquin, M., Delit, A., Wuscher, N., Debeaupuis, J.P., Huerre, M., and Latge, J.P. (1996). Attenuated virulence of uridine-uracil auxotrophs of *Aspergillus fumigatus*. *Infect. Immun.* 64, 4401–4405.

- Escoffre, J.M., Portet, T., Wasungu, L., Teissié, J., Dean, D., and Rols, M.P. (2009). What is (still not) known of the mechanism by which electroporation mediates gene transfer and expression in cells and tissues. *Mol. Biotechnol.* *41*, 286–295.
- Gebremariam, T., Alkhazraji, S., Soliman, S.S.M., Gu, Y., Jeon, H.H., Zhang, L., French, S.W., Stevens, D.A., Edwards, J.E., Filler, S.G., et al. (2019). Anti-CotH3 antibodies protect mice from mucormycosis by prevention of invasion and augmenting opsonophagocytosis. *Sci. Adv.* *5*, eaaw1327.
- Gruber, F., Visser, J., Kubicek, C.P., and de Graaff, L.H. (1990). The development of a heterologous transformation system for the cellulolytic fungus *Trichoderma reesei* based on a pyrG-negative mutant strain. *Curr. Genet.* *18*, 71–76.
- Gupta, A., and Chattoo, B.B. (2007). A novel gene MGA1 is required for appressorium formation in *Magnaporthe grisea*. *Fungal Genet. Biol.* *44*, 1157–1169.
- Gutiérrez, A., López-García, S., and Garre, V. (2011). High reliability transformation of the basal fungus *Mucor circinelloides* by electroporation. *J. Microbiol. Methods* *84*, 442–446.
- Hassan, M.I.A., and Voigt, K. (2019). Pathogenicity patterns of mucormycosis: Epidemiology, interaction with immune cells and virulence factors. *Med. Mycol.* *57*, S245–S256.
- Ibragimova, S., Szebenyi, C., Sinka, R., Alzyoud, E.I., Homa, M., Vágvölgyi, C., Nagy, G., and Papp, T. (2020). CRISPR-Cas9-based mutagenesis of the mucormycosis-causing fungus *Lichtheimia corymbifera*. *Int. J. Mol. Sci.* *21*, 1–11.
- Ibrahim, A.S., Gebremariam, T., Fu, Y., Lin, L., Husseiny, M.I., French, S.W., Schwartz, J., Skory, C.D., Edwards, J.E., and Spellberg, B.J. (2007). The iron chelator deferasirox protects mice from mucormycosis through iron starvation. *J. Clin. Invest.* *117*, 2649–2657.
- Ibrahim, A.S., Gebremariam, T., Lin, L., Luo, G., Husseiny, M.I., Skory, C.D., Fu, Y., French, S.W., Edwards, J.E., Jr., and Spellberg, B. (2010). The high affinity iron permease is a key virulence factor required for *Rhizopus oryzae* pathogenesis. *Mol. Microbiol.* *77*, 587–604.
- Jeong, W., Keighley, C., Wolfe, R., Lee, W.L., Slavin, M.A., Kong, D.C.M., and Chen, S.C.-A. (2019). The epidemiology and clinical manifestations of mucormycosis: A systematic review and meta-analysis of case reports. *Clin. Microbiol. Infect.* *25*, 26–34.
- John, T.M., Jacob, C.N., and Kontoyiannis, D.P. (2021). When uncontrolled diabetes mellitus and severe COVID-19 converge: The perfect storm for mucormycosis. *J. Fungi* *7*, 298.
- Kontoyiannis, D.P. (2017). Antifungal resistance: An emerging reality and a global challenge. *J. Infect. Dis.* *216*, S431–S435.
- Lasker, B.A., and Borgia, P.T. (1980). High-frequency heterokaryon formation by *Mucor racemosus*. *J. Bacteriol.* *141*, 565–569.
- Lastovetsky, O.A., Gaspar, M.L., Mondo, S.J., LaButti, K.M., Sandor, L., Grigoriev, I.V., Henry, S.A., and Pawlowska, T.E. (2016). Lipid metabolic changes in an early divergent fungus govern the establishment of a mutualistic symbiosis with endobacteria. *Proc. Natl. Acad. Sci. USA* *113*, 15102–15107.
- Lax, C., Pérez-arques, C., Navarro-mendoza, M.I., Cánovas-márquez, J.T., Tahiri, G., Pérez-ruiz, J.A., Osorio-concepción, M., Murcia-flores, L., Navarro, E., Garre, V., et al. (2020). Genes, pathways, and mechanisms involved in the virulence of mucorales. *Genes (Basel)* *11*, 317.
- Li, C.H., Cervantes, M., Springer, D.J., Boekhout, T., Ruiz-Vazquez, R.M., Torres-Martinez, S.R., Heitman, J., and Lee, S.C. (2011). Sporangiospore size dimorphism is linked to virulence of *Mucor circinelloides*. *PLoS Pathog.* *7*, e1002086.
- López-Fernández, L., Sanchis, M., Navarro-Rodríguez, P., Nicolás, F.E., Silva-Franco, F., Guarro, J., Garre, V., Navarro-Mendoza, M.I., Pérez-Arques, C., and Capilla, J. (2018). Understanding *Mucor circinelloides* pathogenesis by comparative genomics and phenotypical studies. *Virulence* *9*, 707–720.
- López-Muñoz, A., Nicolás, F.E., García-Moreno, D., Pérez-Oliva, A.B., Navarro-Mendoza, M.I., Hernández-Oñate, M.A., Herrera-Estrella, A., Torres-Martínez, S., Ruiz-Vázquez, R.M., Garre, V., et al. (2018). An adult zebrafish model reveals that mucormycosis induces apoptosis of infected macrophages. *Sci. Rep.* *8*, 12802.
- Luo, G., Gebremariam, T., Lee, H., French, S.W., Wiederhold, N.P., Patterson, T.F., Filler, S.G., and Ibrahim, A.S. (2013). Efficacy of liposomal amphotericin B and posaconazole in intratracheal models of murine mucormycosis. *Antimicrob. Agents Chemother.* *57*, 3340–3347.
- Maurer, E., Binder, U., Sparber, M., Lackner, M., Caramalho, R., and Lass-Flörl, C. (2015). Susceptibility profiles of amphotericin B and posaconazole against clinically relevant Mucorales species under hypoxic conditions. *Antimicrob. Agents Chemother.* *59*, 1344–1346.
- Mondo, S.J., Lastovetsky, O.A., Gaspar, M.L., Schwardt, N.H., Barber, C.C., Riley, R., Sun, H., Grigoriev, I.V., and Pawlowska, T.E. (2017). Bacterial endosymbionts influence host sexuality and reveal reproductive genes of early divergent fungi. *Nat. Commun.* *8*, 1843.
- Navarro, E., Lorca-Pascual, J., Quiles-Rosillo, M., Nicolás, F., Garre, V., Torres-Martínez, S., and Ruiz-Vázquez, R. (2001). A negative regulator of light-inducible carotenogenesis in *Mucor circinelloides*. *Mol. Genet. Genomics* *266*, 463–470.
- Navarro, E., Peñaranda, A., Hansberg, W., Torres-Martínez, S., and Garre, V. (2013). A White Collar 1-like protein mediates opposite regulatory functions in *Mucor circinelloides*. *Fungal Genet. Biol.* *52*, 42–52.
- Navarro-Mendoza, M.I., Pérez-Arques, C., Murcia, L., Martínez-García, P., Lax, C., Sanchis, M., Capilla, J., Nicolás, F.E., and Garre, V. (2018). Components of a new gene family of ferroxidases involved in virulence are functionally specialized in fungal dimorphism. *Sci. Rep.* *8*, 7660.
- Navarro-Mendoza, M.I., Pérez-Arques, C., Panchal, S., Nicolás, F.E., Mondo, S.J., Ganguly, P., Pangilinan, J., Grigoriev, I.V., Heitman, J., Sanyal, K., et al. (2019). Early diverging fungus *Mucor circinelloides* lacks centromeric histone CENP-A and displays a mosaic of point and regional centromeres. *Curr. Biol.* *29*, 3791–3802.e6.
- Nicolas, F.E., Torres-Martínez, S., and Ruiz-Vázquez, R.M. (2003). Two classes of small antisense RNAs in fungal RNA silencing triggered by non-integrative transgenes. *EMBO J.* *22*, 3983–3991.
- Nicolas, F.E., de Haro, J.P., Torres-Martínez, S., and Ruiz-Vazquez, R.M. (2007). Mutants defective in a *Mucor circinelloides* dicer-like gene are not compromised in siRNA silencing but display developmental defects. *Fungal Genet. Biol.* *44*, 504–516.
- Nicolas, F.E., Calo, S., Murcia-Flores, L., Garre, V., Ruiz-Vazquez, R.M., and Torres-Martínez, S. (2008). A RING-finger photocarotenogenic repressor involved in asexual sporulation in *Mucor circinelloides*. *FEMS Microbiol. Lett.* *280*, 81–88.
- Nicolás, F.E., Navarro-Mendoza, M.I., Pérez-Arques, C., López-García, S., Navarro, E., Torres-Martínez, S., and Garre, V. (2018). Molecular tools for carotenogenesis analysis in the mucoral *Mucor circinelloides*. In *Methods in Molecular Biology* (Humana Press Inc.), pp. 221–237.
- Nicolás-Molina, F.E., Navarro, E., and Ruiz-Vázquez, R.M. (2008). Lycopene over-accumulation by disruption of the negative regulator gene *crgA* in *Mucor circinelloides*. *Appl. Microbiol. Biotechnol.* *78*, 131–137.
- Nosheen, S., Yang, J., Naz, T., Nazir, Y., Ahmad, M.I., Fazili, A.B.A., Li, S., Mustafa, K., and Song, Y. (2021). Annotation of AMP-activated protein kinase genes and its comparative transcriptional analysis between high and low lipid producing strains of *Mucor circinelloides*. *Biotechnol. Lett.* *43*, 193–202.
- Obraztsova, I.N., Prados, N., Holzmann, K., Avalos, J., and Cerdá-Olmedo, E. (2004). Genetic damage following introduction of DNA in Phycormycetes. *Fungal Genet. Biol.* *41*, 168–180.
- Ozturk, D.H., Dorfman, R.H., Scapin, G., Sacchetti, J.C., and Grubmeyer, C. (1995). Locations and functional roles of conserved lysine residues in Salmonella typhimurium orotate phosphoribosyltransferase. *Biochemistry* *34*, 10755–10763.
- Patiño-Medina, J.A., Maldonado-Herrera, G., Pérez-Arques, C., Alejandre-Castañeda, V., Reyes-Mares, N.Y., Valle-Maldonado, M.I., Campos-García, J., Ortiz-Alvarado, R., Jácome-Galarza, I.E., Ramírez-Díaz, M.I., et al. (2018).

Control of morphology and virulence by ADP-ribosylation factors (Arf) in *Mucor circinelloides*. *Curr. Genet.* *64*, 853–869.

Patiño-Medina, J.A., Reyes-Mares, N.Y., Valle-Maldonado, M.I., Jácome-Galarza, I.E., Pérez-Arques, C., Nuñez-Anita, R.E., Campos-García, J., Anaya-Martínez, V., Ortiz-Alvarado, R., Ramírez-Díaz, M.I., et al. (2019). Heterotrimeric G-alpha subunits Gpa11 and Gpa12 define a transduction pathway that control spore size and virulence in *Mucor circinelloides*. *PLoS One* *14*, e0226682.

Peng, D., and Tarleton, R. (2015). (2015). EuPaGDT: a web tool tailored to design CRISPR guide RNAs for eukaryotic pathogens. *Microb Genomics* *1*.

Pérez-Arques, C., Navarro-Mendoza, M.I., Murcia, L., Lax, C., Martínez-García, P., Heitman, J., Nicolás, F.E., and Garre, V. (2019). *Mucor circinelloides* thrives inside the phagosome through an Atf-mediated germination pathway. *mBio* *10*, 1–15.

Pérez-Arques, C., Navarro-Mendoza, M.I., Murcia, L., Navarro, E., Garre, V., and Nicolás, F.E. (2021a). The RNAi mechanism regulates a new Exonuclease gene involved in the virulence of mucorales. *Int. J. Mol. Sci.* *22*, 2282.

Pérez-Arques, C., Navarro-Mendoza, M.I., Murcia, L., Lax, C., Sanchis, M., Capilla, J., Navarro, E., Garre, V., and Nicolás, F.E. (2021b). A mucoralean white collar-1 photoreceptor controls virulence by regulating an intricate gene network during host interactions. *Microorganisms* *9*, 459.

Prakash, H., and Chakrabarti, A. (2019). Global epidemiology of mucormycosis. *J. Fungi* *5*, 26.

Roden, M.M., Zoutis, T.E., Buchanan, W.L., Knudsen, T.A., Sarkisova, T.A., Schaufele, R.L., Sein, M., Sein, T., Chiou, C.C., Chu, J.H., et al. (2005). Epidemiology and outcome of zygomycosis: A review of 929 reported cases. *Clin. Infect. Dis.* *41*, 634–653.

Roncero, M.I.G., Jepsen, L.P., Ströman, P., and van Heeswijck, R. (1989). Characterization of a *leuA* gene and an ARS element from *Mucor circinelloides*. *Gene* *84*, 335–343.

Saha, P., Ghosh, S., and Roy-Barman, S. (2020). MoLAEA regulates secondary metabolism in *Magnaporthe oryzae*. *mSphere* *5*, e00936.

Scapin, G., Ozturk, D.H., Grubmeyer, C., and Sacchettini, J.C. (1995). The crystal structure of the orotate phosphoribosyltransferase complexed with orotate and α -D-5-Phosphoribosyl-1-pyrophosphate. *Biochemistry* *34*, 10744–10754.

Schneider, Caroline A., Rasband, Wayne S., and Eliceiri, Kevin W. (2012). NIH Image to ImageJ: 25 years of image analysis. *Nat. Methods* *9*, 671–675.

Silva, F., Navarro, E., Peñaranda, A., Murcia-Flores, L., Torres-Martínez, S., and Garre, V. (2008). A RING-finger protein regulates carotenogenesis via proteolysis-independent ubiquitylation of a White Collar-1-like activator. *Mol. Microbiol.* *70*, 1026–1036.

Skiada, A., Pagano, L., Groll, A., Zimmerli, S., Dupont, B., Lagrou, K., Lass-Flori, C., Bouza, E., Klimko, N., Gaustad, P., et al. (2011). Zygomycosis in Europe: Analysis of 230 cases accrued by the registry of the European confederation of medical mycology (ECMM) working group on zygomycosis between 2005 and 2007. *Clin. Microbiol. Infect.* *17*, 1859–1867.

Soliman, S.S.M., Hamdy, R., Elseginy, S.A., Gebremariam, T., Hamoda, A.M., Madkour, M., Venkatachalam, T., Ershaid, M.N., Mohammad, M.G., Chamilos, G., et al. (2020). Selective inhibition of *Rhizopus eumelanin* biosynthesis by novel natural product scaffold-based designs caused significant inhibition of fungal pathogenesis. *Biochem. J.* *477*, 2489–2507.

Soliman, S.S.M., Baldin, C., Gu, Y., Singh, S., Gebremariam, T., Swidergall, M., Alqarihi, A., Youssef, E.G., Alkhazraji, S., Pikoulas, A., et al. (2021). Mucorin is a ricin-like toxin that is critical for the pathogenesis of mucormycosis. *Nat. Microbiol.* *6*, 313–326.

Sridhara, S.R., Paragache, G., Panda, N.K., and Chakrabarti, A. (2005). Mucormycosis in immunocompetent individuals: An increasing trend. *J. Otolaryngol.* *34*, 402–406.

Trieu, T.A., Calo, S., Nicolás, F.E., Vila, A., Moxon, S., Dalmay, T., Torres-Martínez, S., Garre, V., and Ruiz-Vázquez, R.M. (2015). A non-canonical RNA silencing pathway promotes mRNA degradation in basal fungi. *PLoS Genet.* *11*, e1005168.

Trieu, T.A., Navarro-Mendoza, M.I., Pérez-Arques, C., Sanchis, M., Capilla, J., Navarro-Rodríguez, P., Lopez-Fernandez, L., Torres-Martínez, S., Garre, V., Ruiz-Vázquez, R.M., et al. (2017). RNAi-based functional genomics identifies new virulence determinants in mucormycosis. *PLoS Pathog.* *13*, e1006150.

van Heeswijck, R., and Roncero, M.I.G. (1984). High frequency transformation of *Mucor* with recombinant plasmid DNA. *Carlsberg Res. Commun.* *49*, 691.

Valle-Maldonado, M.I., Patiño-Medina, J.A., Pérez-Arques, C., Reyes-Mares, N.Y., Jácome-Galarza, I.E., Ortiz-Alvarado, R., Vellanki, S., Ramírez-Díaz, M.I., Lee, S.C., Garre, V., et al. (2020). The heterotrimeric G-protein beta subunit Gpb1 controls hyphal growth under low oxygen conditions through the protein kinase A pathway and is essential for virulence in the fungus *Mucor circinelloides*. *Cell. Microbiol.* *22*, e13236.

Veisi, A., Bagheri, A., Eshaghi, M., Rikhtehgar, M.H., Rezaei Kanavi, M., and Farjad, R. (2021). Rhino-orbital mucormycosis during steroid therapy in COVID-19 patients: A case report. *Eur. J. Ophthalmol.* <https://doi.org/10.1177/11206721211009450>.

Vellanki, S., Navarro-Mendoza, M.I., Garcia, A., Murcia, L., Pérez-Arques, C., Garre, V., Nicolás, F.E., and Lee, S.C. (2018). *Mucor circinelloides*: Growth, maintenance, and genetic manipulation. *Curr. Protoc. Microbiol.* *49*, e53.

von Arx, J.A., and Schipper, M.A.A. (1978). The CBS fungus collection. *Adv. Appl. Microbiol.* *24*, 215–236.

Wagner, L., Stielow, J.B., de Hoog, G.S., Bensch, K., Schwartze, V.U., Voigt, K., Alastruey-Izquierdo, A., Kurzai, O., and Walther, G. (2020). A new species concept for the clinically relevant *Mucor circinelloides* complex. *Persoonia* *44*, 67–97.

Yuzbashev, T.V., Larina, A.S., Vybornaya, T.V., Yuzbasheva, E.Y., Gvilava, I.T., and Sineoky, S.P. (2015). Repetitive genomic sequences as a substrate for homologous integration in the *Rhizopus oryzae* genome. *Fungal Biol.* *119*, 494–502.

STAR★METHODS

KEY RESOURCES TABLE

REAGENT or RESOURCE	SOURCE	IDENTIFIER
Bacterial and virus strains		
<i>Escherichia coli</i> Dh5 α	Thermo Fisher Scientific	N/A
Chemicals, peptides, and recombinant proteins		
Uridine	Merck KGaA	Cat#U3003
L-Leucine	Merck KGaA	Cat#L8000
5 Fluoroorotic acid monohydrate (5-FOA)	Apollo Scientific	Cat#PC4054
EDTA	Merck KGaA	Cat#EDS
Tris	Merck KGaA	Cat#T1503
Niacine (nicotinic acid)	Merck KGaA	Cat#N0761
Thiamine	Merck KGaA	Cat#T1270
D-Sorbitol	Merck KGaA	Cat#S1876
Lysing Enzymes	Merck KGaA	Cat#L412
Chitosanase	Merck KGaA	Cat#C9830
DMSO	Merck KGaA	Cat#D8418
SDS	Merck KGaA	Cat#L3771
RNase A	Merck KGaA	Cat#R6513
Phenol	Merck KGaA	Cat#P1037
Chloroform	Merck KGaA	Cat#C2432
Isoamyl alcohol	Merck KGaA	Cat#309435
Ammonium acetate	Merck KGaA	Cat#A1542
Ethanol	Merck KGaA	Cat#51976
Hydrochloric acid	Merck KGaA	Cat#H1758
Critical commercial assays		
Alt-R™ CRISPR-Cas9 crRNA	IDT	See Table S1
Alt-R™ CRISPR-Cas9 tracrRNA	IDT	Cat#1072533
Alt-R™ S.p. Cas9 Nuclease V3	IDT	Cat#1081058
Deposited data		
Mucoromycotina genomes	Joint Genome Institute MycoCosm	https://mycoCosm.jgi.doe.gov/mucoromycotina/mucoromycotina_info.html
<i>R. microsporus pyrG</i>	Joint Genome Institute MycoCosm	<i>R. microsporus</i> Protein ID 279857
<i>R. microsporus pyrF</i>	Joint Genome Institute MycoCosm	<i>R. microsporus</i> Protein ID 231940
<i>R. microsporus leuA</i>	Joint Genome Institute MycoCosm	<i>R. microsporus</i> Protein ID 228594
<i>R. microsporus crgA</i>	Joint Genome Institute MycoCosm	<i>R. microsporus</i> Protein ID 226533
Experimental models: Organisms/strains		
<i>Rhizopus microsporus</i> ATCC 11559	Kindly provided by Dr. Teresa E. Pawlowska (Cornell University)	N/A
<i>Rhizopus microsporus</i> UM1: <i>pyrF</i>	This Study	N/A
<i>Rhizopus microsporus</i> UM3: <i>crgA::pyrF</i>	This Study	N/A
<i>Rhizopus microsporus</i> UM4: <i>crgA::pyrF</i>	This Study	N/A
<i>Rhizopus microsporus</i> UM6: <i>leuA::pyrF</i>	This Study	N/A
<i>Rhizopus microsporus</i> UM7: <i>leuA::pyrF</i>	This Study	N/A
<i>Mucor lusitanicus</i> CBS 277.49	von Arx and Schipper, 1978	N/A
<i>Mucor lusitanicus</i> MU223: <i>crgAΔ::pyrG</i>	Silva et al., 2008	N/A

(Continued on next page)

Continued		
REAGENT or RESOURCE	SOURCE	IDENTIFIER
Oligonucleotides		
Oligonucleotides	This Study	See Table S1
Recombinant DNA		
pBluescript II SK+	Agilent	Cat#212205
pMAT1819	This Study	N/A
Software and algorithms		
Snapgene v5.1.0	Snapgene Software	https://www.snapgene.com/
EuPaGDT	Peng and Tarleton, 2015	http://gma.ctegd.uga.edu/
NIS Elements Software	Nikon	https://www.microscope.healthcare.nikon.com/products/software/nis-elements
ImageJ v1.51m9	Schneider et al., 2012	
Zeiss Zen v2.5	Zeiss	https://www.zeiss.com/microscopy/us/products/microscope-software/zen.html#introduction
Jmol		http://jmol.sourceforge.net/
Mol*		http://molstar.org
GraphPad Prism v8.0.2	Graphpad Software	https://www.graphpad.com/
IBM SPSS Statistic	IBM Software	https://www.ibm.com/analytics/spss-statistics-software

RESOURCE AVAILABILITY

Lead contact

Further information and requests for resources and reagents should be directed to and fulfilled by the lead contact, Victoriano Garre (vgarre@umes.es).

Materials availability

All plasmids and fungal strains generated in this study are available from the lead contact without restriction.

Data and code availability

- All data reported in this paper will be shared by the lead contact upon request.
- This paper does not report original code.
- Any additional information required to reanalyze the data reported in this paper is available from the lead contact upon request.

EXPERIMENTAL MODEL AND SUBJECT DETAILS

All the fungal strains used and generated in this work derive from *Rhizopus microsporus* ATCC 11559 and *M. circinelloides* CBS277.49. Uridine and leucine auxotrophies were checked in the minimal media yeast nitrogen base, YNB ([Lasker and Borgia, 1980](#)). When specified, media was supplemented with uridine (200 mg/L) or leucine (20 mg/L). Transformants of the auxotrophic strain UM1 strain with the *pyrF* complementation plasmid or the *pyrF* template used in CRISPR/Cas9 disruption experiments were grown in Minimal Media with Casamino acids (MMC) ([Nicolas et al., 2007](#)). Electroporated protoplasts were resuspended in ice-cold YPG media + 0.5 M Sorbitol for 90 min and then centrifuged at 800 rpm and resuspended in YNB media + 0.5 M Sorbitol. The resuspended protoplasts were plated in MMC + 0.5 M Sorbitol media to select transformants. All strains were grown at 30°C. *Escherichia coli* strain DH5 α (Thermo Fisher Scientific) was used for all cloning experiments.

METHODS DETAILS

Protoplast generation and electroporation

A total of 1×10^7 spores/mL were inoculated in 25 mL liquid YPG media and preincubated overnight at 4°C in YPG media supplemented with 200 mg/L of uridine. The culture was incubated at 33°C for approximately 4 hours and 30 min at 250 rpm in a rotary shaker. When spores reached the optimal germination stage, the culture was centrifuged, and the spores were washed twice with PS buffer (1X PBS and 0.5M Sorbitol) and resuspended in 5 mL of PS buffer. To digest the cell wall, 3 mg of lysing enzymes

from *Trichoderma harzianum* (Merck KGaA, Darmstadt, Germany) and 0.0008 units of Chitosanase from *Streptomyces griseus* (Merck KGaA, Darmstadt, Germany) were added to the resuspended germinules. The digestion was incubated at 30°C for 90 min at 60 rpm in a rotary shaker. Protoplasts were washed twice with ice-cold 0.5 M sorbitol and transferred to 0.2 cm electroporation cuvettes (Fisher Scientific, FB102). Up to 20 μ l of pMAT1819 (1–4 μ g of DNA) or gRNA-Cas9 complex (see gRNA-Cas9 assembly and *in vitro* activity tests) and up to 20 μ l of purified template DNA (0.5–4 μ g of DNA) were added and mixed with 200 μ l of protoplasts. After the electroporation pulses, applied with Gene Pulser XCell (Biorad, Hercules, California, USA), protoplasts were rapidly resuspended in YPG + 0.5 M sorbitol. When survival rates of the protoplasts were analyzed, 10 μ l of pulsed protoplasts were diluted in 90 μ l of 0.5 M sorbitol, and an aliquot was counted in a Neubauer chamber to determine concentration. Then, two hundred protoplasts were plated on minimal media (MMC) supplemented with uridine (200 mg/L) (two plates/cuvette). As a control, two hundred protoplasts that did not undergo electroporation were also plated in the same medium. The same procedure was followed to determine the effect of germination temperature on protoplasts viability. pMAT1819 plasmid was used in CRISPR/Cas9 disruption experiments as a positive control of the transformation/electroporation efficiency, while no DNA was added in negative controls.

Transformation efficiency score was obtained as the product of the average transformants/ μ g of DNA and the average survival rate (normalized considering 1 as the value of the survival rate of the negative control).

Nucleic acids manipulation, amplification, and plasmid construction

DNA from *R. microsporus* was extracted following a chloroform/phenol protocol. Briefly, mycelia were quickly frozen in liquid nitrogen and then ground using mortar and pestle. 200 to 500 mg of the resulting powder was treated with Extraction Buffer (Tris-HCl 200 mM, EDTA 100 mM and 1% SDS), RNase A (10 mg/mL), and 1 mL of phenol pH 8.0. After mixing and centrifuge, the aqueous phase was washed three times using 1/2 volume of phenol pH 8 and 1/2 volume of isoamyl alcohol:chloroform (24:1). The aqueous phase was treated again with 1 volume of isoamyl alcohol:chloroform and then transferred to a different tube and mixed with 1/10 volume of 5 M ammonium acetate and 1 volume of ice-cold ethanol. The DNA pellet was washed with 1 mL of 80% ethanol. The supernatant was discarded, and the DNA was dried at room temperature for 10 min. Finally, DNA was resuspended with ultrapure water. All PCRs amplifications were performed with the Herculase II Fusion DNA polymerase (Agilent, Santa Clara, California, USA), adapting annealing temperature to each primer pair following the manufacturer's recommendations. DNA templates and fragments for crRNAs in *in vitro* test were purified using GeneJet PCR Purification Kit (Thermo Scientific).

To construct the plasmid pMAT1819 to complement *pyrF* mutation, we first PCR amplified the 4.2-kb *pyrF* locus from the wild-type DNA using the primers *pyrF_F_EcoRI* and *pyrF_R_XhoI*, which have the indicated restriction sites at their 5' end (Table S1). The *pyrF* fragment in this plasmid included a 2357-bp sequence upstream the translation start codon and 1010-bp sequence downstream the stop codon of the gene to ensure that the construction contained the promoter and terminator of the *pyrF* gene. The pBluescript SK(+) vector was double digested using the *EcoRI* and *XhoI* restriction enzymes, and the 4.2-kb *pyrF* fragment was ligated at room temperature using T4 ligase (Thermo Scientific, Waltham, Massachusetts, USA). Electrocompetent cells of *Escherichia coli* (DH5 α) were transformed and plated in LB media supplemented with ampicillin (100 mg/L). The plasmid was extracted from colonies using the GeneJet Plasmid Miniprep Kit (Thermo Scientific, Waltham, Massachusetts, USA) and checked by digestion followed to electrophoresis and sequenced with *pyrF_F_SEQ* and *pyrF_R_SEQ* (Table S1). Sequencing was performed with a 3500 Genetic Analyzer (Thermo Scientific, Waltham, Massachusetts, USA).

Selection of uracil auxotrophic mutants

After 4–5 days of growth in solid YPG media, 1×10^7 spores were collected, washed, and inoculated in 200 mL of liquid YPG media supplemented with 3 g/L of 5-FOA and 200 mg/L uridine. After 48 hours of growth at 30°C in a rotary shaker (250 rpm), the complete culture was centrifuged, and the pellet was plated on solid YPG media plates, also supplemented with 3 g/L of 5-FOA and 200 mg/L uridine. After 24 hours, resistant colonies were isolated and plated again on solid YPG media supplemented with 3 g/L of 5-FOA and 200 mg/L of uridine. The colonies showing a robust growth were plated on solid YNB media with and without uridine (200 mg/L). DNA from the colonies resistant to 5-FOA and unable to grow without uridine was extracted. The *pyrG* gene and the *pyrF* gene were PCR amplified using the primers *pyrF_F_SEQ* and *pyrF_R_SEQ* (*pyrF*) and *pyrG_F_SEQ* and *pyrG_R_SEQ* (*pyrG*) (Table S1) and sequenced. The sequences of the *pyrG* and *pyrF* genes were aligned to the wild-type sequences available at JGI MycoCosm portal (<https://mycocosm.jgi.doe.gov>) (Lastovetsky et al., 2016) using SnapGene® software (from GSL Biotech; available at snapgene.com).

gRNA – Cas9 assembly and *in vitro* activity tests

Targeted gene disruption and *in vitro* activity tests required the ribonucleoprotein (gRNA – Cas9) complex assembly. Alt-R™ CRISPR-Cas9 crRNA, Alt-R™ CRISPR-Cas9 tracrRNA, and Alt-R™ S.p. Cas9 Nuclease were purchased from IDT (<https://www.idtdna.com/site/order/oligoentry/index/crispr>). The tracrRNA and crRNA were assembled to generate de gRNA following the manufacturer's recommendations and the protocol developed for *Aspergillus fumigatus* (Abdallah et al., 2017). Briefly, we used a 33 μ M equimolecular mix of crRNA, tracrRNA (common to every crRNA), and Nuclease-Free Duplex Buffer (IDT). The mix was incubated at 95°C for 5 min and cooled down at room temperature. 1.5 μ l per electroporation cuvette of gRNA were mixed with 0.075 μ g of Cas9 and 11 μ l of PBS 1X. The mix was left for 5–10 min at room temperature before the electroporation to allow ribonucleoprotein complex assembly. 20-nt protospacer sequences were designed using the genome of *R. microsporus* (<https://mycocosm.jgi.doe.gov>)

(Lastovetsky et al., 2016) and the tool EuPaGDT (Eukaryotic Pathogen CRISPR guide RNA/DNA Design Tool) with recommended default settings (Peng and Tarleton, 2015). The crRNAs were purchased from IDT (<https://eu.idtdna.com/site/order/oligoentry/index/crispr>, IDT, Coralville, IA, USA) (Table S1). For *in vitro* activity assays, gRNA (crRNA and tracrRNA) and the ribonucleoprotein complex were assembled following the same procedure mentioned above. Subsequently, the gRNA, Cas9, and 100–400 ng of DNA were incubated at 30°C for 2 hours. The DNA corresponding to the wild-type loci were PCR amplified, using the Up_F primer and the Dw_R primer (Table S1), and purified using the Gene Jet PCR Purification Kit (Thermo Scientific, Waltham, Massachusetts, USA). Negative controls contained the same mix except for the crRNA. The *in vitro* reaction was inactivated (65°C for 20 min), and the cleavage products were separated by agarose gel electrophoresis (0.7%).

Phenotypic characterization of *crgA* and *leuA* mutants

For radial growth and spore production analysis, a drop with 1×10^3 spores was inoculated in the center of a plate. For radial growth, diameter measures were taken after 24, 48, and 72 hours. For spore production, a chunk of agar of 1 cm² (one per plate, three for each strain and time) was transferred to a 50 ml tube containing 10 mL of PBS 1X. The tube was vigorously vortexed to release spores. Spores were counted in a Neubauer chamber to determine the concentration, and total spore production was calculated. For total melanin quantification, 20 mg of lyophilized biomass was crushed and resuspended in 0.5 mL of a 1 N NaOH solution + 10 % DMSO. Samples were incubated at 80°C for 1 hour and vortex every 5–10 min. After centrifugation, the absorbance of the supernatants was measured at 405 nm (Gupta and Chattoo, 2007; Saha et al., 2020). For leucine auxotrophy analysis, small pieces of mycelium were plated in minimal YNB and YNB media supplemented with leucine (20 mg/l), and the growth (or its absence) observed after 48 hours.

Microscopy imaging, data representation, and statistical analysis

For the germination experiments, 15 μ l of spores or germinated spores were placed on a slide and covered with a coverslip. Images of germinated spores were acquired with a Nikon Eclipse 80i microscopy equipped with a Nikon DS-Ri2 camera and processed with NIS Elements Software and ImageJ (Schneider et al., 2012). Microscopy images showing the mycelia and growth differences (Figure 4) were obtained using a Stemi 305 Zeiss microscope (integrated camera). Schematic illustrations of the orotate phosphoribosyl transferase structure were obtained using the available structure of the *S. typhimurium* enzyme (PDB: 1OPR, (Ozturk et al., 1995; Scapin et al., 1995), using Jmol (<http://jmol.sourceforge.net/>) and Mol* (<http://molstar.org>).

Survival assays

Male Swiss mice weighing 30 g and one-month-old (Animal Facilities Services, University of Murcia, Spain) were used as an animal model for virulence assays. The mice were kept in groups of 8 individuals per cage. The infection was initiated one week later by forming the groups, letting a stable hierarchy and no conflict in the group. Mice were injected intravenously by retroorbital injection of $1 \cdot 10^6$ spores (Chang and Heitman, 2019). Isoflurane anesthetic was used during the procedure to ensure animal welfare, and the mice were monitored after the procedure until full recovery from the anesthesia. Mice were maintained in established conditions with free food, autoclaved water, and continuous ventilation. The animal welfare was checked twice a day for 15 days, and mice following the discomfort criteria were euthanized in a CO₂ chamber. Survival rates were plotted in a Kaplan–Meier curve (GraphPad Prism), and differences were considered statistically significant with a p-value ≤ 0.05 in a Mantel–Cox test. To guarantee the welfare of the animals and the ethics of any procedure related to animal experimentation, all the experiments performed in this work comply with the Guidelines of the European Union Council (Directive 2010/63/EU) and the Spanish RD 53/2013. Experiments and procedures were supervised and approved by the University of Murcia Animal Welfare and Ethics Committee and the Council of Water, Agriculture, Farming, Fishing and Environment of Murcia (Consejería de Agua, Agricultura, Ganadería, Pesca y Medio Ambiente de la CARM), Spain (authorization number REGA ES300305440012).

QUANTIFICATION AND STATISTICAL ANALYSIS

For the graphical representation of data, GraphPad Prism version 8.0.2 for Windows was used (GraphPad Software, San Diego, California USA, www.graphpad.com). Radial growth and spore production results were expressed as mean \pm S.E. The data were analyzed with the software IBM SPSS Statistic for Mac [IBM Corp (2014) Version 23.0.; <https://www.ibm.com/SPSS-Statistics/>]. An ANOVA of a single factor was used to determine statistically significant differences between the wild type strain and the mutants, assuming a significance level of 95% (P-value < 0.05), followed by the Tuckey or Games Howell tests, according to the homogeneity of the variables.

Cell Reports Methods, Volume 1

Supplemental information

**Stable and reproducible homologous
recombination enables CRISPR-based engineering
in the fungus *Rhizopus microsporus***

Carlos Lax, María Isabel Navarro-Mendoza, Carlos Pérez-Arques, Eusebio Navarro, Francisco Esteban Nicolás, and Victoriano Garre

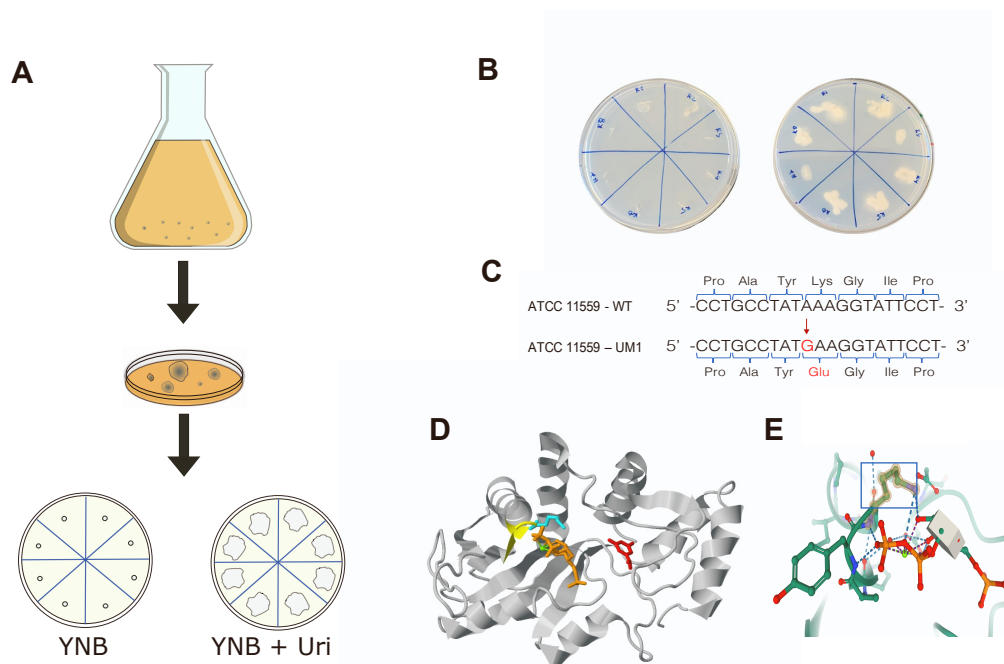


Figure S1. Generation of the uridine auxotrophic strain UM1 and mutation characterization, Related to STAR Methods. (A) Schematic representation of the workflow followed to isolate uracil auxotrophic strains. (B) 5-FOA resistant isolates R1-R8 after 24 hours of growth on YNB with (right) and without uridine (left). (C) Nucleotide sequences and encoded amino acids of *pyrF* gene sequence (+207-+227) that differed between the *R. microsporus* wild-type strain ATCC 11559 and the UM1 strain. The nucleotide mutation and the amino acid change found in the UM1 are highlighted in red. (D) Orotate phosphoribosyltransferase (PyrF) structure of *S. typhimurium*. The active site is colored in yellow (71-74), the Lys73 residue is colored in blue, the orotic acid is colored in red, and the PRPP is colored in orange. (E) Representation of the Lys73 residue highlighted in yellow (inside a blue square) and its interactions with PRPP and other residues.

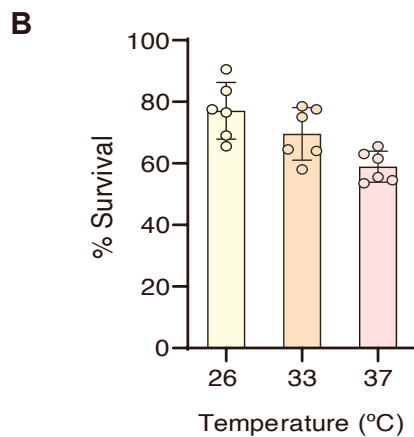
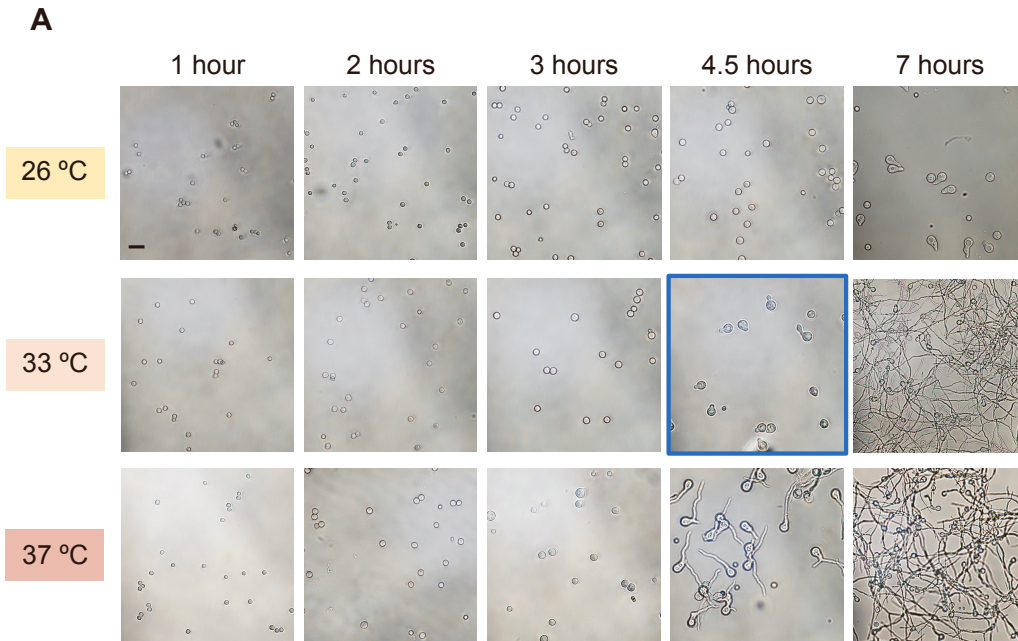


Figure S2. Effect of temperature in germination and protoplast viability, Related to STAR Methods. (A) Germination at 26 °C (top), 33 °C (middle), and 37 °C (above) of the UM1 strain in rich YPG media supplemented with uridine. Images were taken (from left to right) at 1, 2, 3, 4.5, and 7 hours. The optimal germination stage for protoplast generation (33 °C and 4.5 hours) is framed in blue. Scale bar = 20 μ m. (B) Spores of the UM1 strain were germinated at 26 °C, 33 °C, and 37 °C. After cell wall digestion, two hundred protoplasts were plated in minimal media (MMC) supplemented with uridine. Each point corresponds to the calculated percent survival of each plate (6 plates/condition).

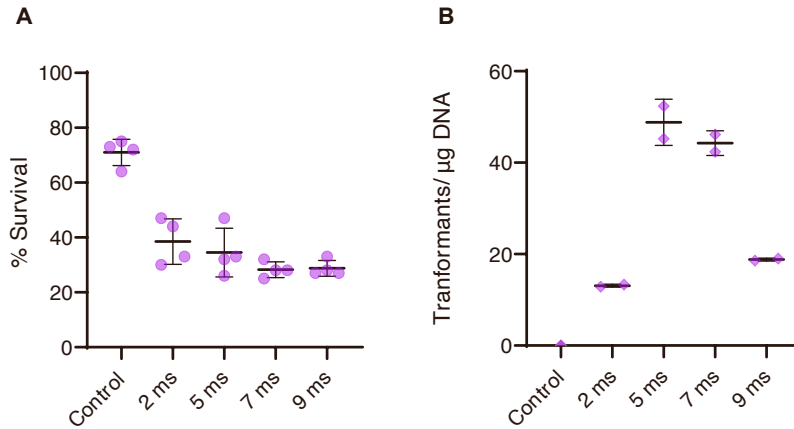


Figure S3. Transformation efficiency and survival rate of electroporation with different pulse duration. Related to Figure 1. (A) The survival rate of UM1 protoplasts after 2, 5, 7, and 9 milliseconds TC pulses. Each point corresponds to a different plate with 200 protoplasts (2 plates/cuvette). **(B)** Transformants/ μg of DNA obtained with 2, 5, 7, and 9 milliseconds TC pulses. Each point corresponds to a different electroporation cuvette.

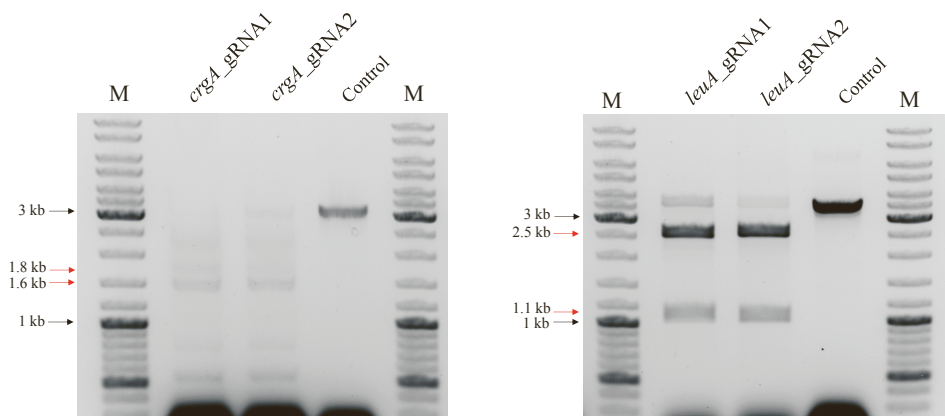


Figure S4. *In vitro* activity test of the crRNAs designed for *crgA* and *leuA* disruption. Related to STAR Methods. PCR amplified *crgA* (left) and *leuA* (right) loci were incubated with Cas9 and gRNA (tracRNA + crRNA) at 30 °C for 2 hours. As a control, crRNA was removed to check unspecific cleaves within the targeted locus. Red arrows point to the expected fragments after the Cas9-gRNA cleave. Black arrows point to the indicated bands of the marker.

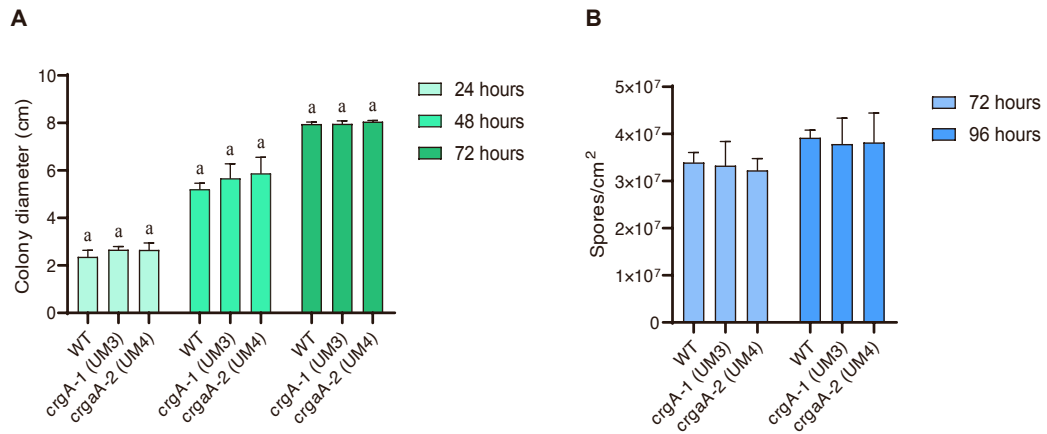


Figure S5. Radial growth analysis and spore production of the *cgrA* mutants UM3 and UM4 compared to the wild-type strain. Related to Figure 4. (A) Colony diameter of *R. microsporius* wild-type strain (WT) and *crgA* mutants UM3 and UM4 after 24, 48, 72 hours of growth in rich YPG media. (B) Total spore production by cm² quantified after 72 and 96 hours. The data were analyzed using one-way ANOVA, and statistical significance is indicated by letters ($p < 0,05$).

Table S1: crRNAs and primers name and sequence used in this work. Related to STAR Methods

crRNA name	Sequence 5'→ 3'
<i>crgA_1</i> (<i>crgA_gRNA1</i>)	GCAAGTGATCCGACCAATAG AGG
<i>crgA_2</i> (<i>crgA_gRNA2</i>)	GCCCGATGGTCGATCGATCG TGG
<i>leuA_1</i> (<i>leuA_gRNA1</i>)	CCTGGCACTACCGTCGTCTG CGG
<i>leuA_2</i> (<i>leuA_gRNA2</i>)	CAAGGTATTGTGCACGTCAT TGG
Primer name	Sequence 5'→ 3'
<i>pyrF_F_SEQ</i>	GGCAATCATGTCATCGGAACT
<i>pyrF_R_SEQ</i>	GCTCAAGGTTGAATAAAGAC
<i>pyrG_F_SEQ</i>	CCCGCATAAATCCTTTTGAA
<i>pyrG_R_SEQ</i>	ACGGACCATTGGATACATCA
<i>pyrF_F_EcoRI</i>	CAGGAATTCGTATCTTGAGCTTACAAACGACTTG
<i>pyrF_R_XhoI</i>	CAGCTCGAGTGATAAACGAAGATGTGGCTGTC
Templ_F_ <i>crgA_1</i>	GATCTTGACCTAGAGCATGATACTCGAGTACCTCTATTCCTCCATAA GAATTTGACAG
Templ_R_ <i>crgA_1</i>	TCATGCAGTTGACTCCAGGGAATGCAAGTGATCCGACCTGATAAAA CGAAGATGTGGCTGTC
Templ_F_ <i>crgA_2</i>	TTGATGCAAGTACAAACCTTGCCCGATGGTCGATCGATTCTCCATA AGAATTTGACAG
Templ_R_ <i>crgA_2</i>	TGGTTACACGAAAGCGATGCGAGCCTACTGCTTCCACGTGATAAAA CGAAGATGTGGCTGTC
Templ_F_ <i>leuA_1</i>	TGAACAAGGATTTACCCTTCTGGCACTACCGTCGTCTTCCTCCATA AGAATTTGACAG
Templ_R_ <i>leuA_1</i>	GCCAAATGCACCATGTGTTGAGGTGTGTGAGTCGCCGC TGATAAACGAAGATGTGGCTGTC
Templ_F_ <i>leuA_2</i>	TGGTATGGAAGATGCTCGTCAAGGTATTGTGCACGTCATCCTCCAT AAGAATTTGACAG
Templ_R_ <i>leuA_2</i>	GGTAGTGCCAGGAAGGGTAAATCCTTGTTGAGGACCAATGATAAAA ACGAAGATGTGGCTGTC
Up_F_ <i>crgA</i>	ATGGCAATAACCAGACCATAACC
Dw_R_ <i>crgA</i>	AACATCCTTCTAGAACCGCGTA
Up_F_ <i>leuA</i>	GCAGCAAAATCCACATAGTCAA
Dw_R_ <i>leuA</i>	CGAAAAAGGAAATAACGCTTTG
<i>pyrF_RC</i>	TAGTCATGCGTCCAGTTTCTGT
M13_F	GTA AACGACGGCCAGT
M13_R	CAGGAAACAGCTATGAC